

12

FG.

Line-By-Line Calculations of Hot-Gas Spectra Including HF and HCl

ADA019573

C. M. RANDALL
Chemistry and Physics Laboratory
Laboratory Operations ✓
The Aerospace Corporation
El Segundo, Calif. 90245

4 December 1975

Interim Report

APPROVED FOR PUBLIC RELEASE:
DISTRIBUTION UNLIMITED

DDC
RECEIVED
JAN 22 1976
RECEIVED
D

Sponsored by
DEFENSE ADVANCED RESEARCH PROJECTS AGENCY
1400 Wilson Blvd, Arlington, Va. 22209

DARPA Order No. 2843

SPACE AND MISSILE SYSTEMS ORGANIZATION
AIR FORCE SYSTEMS COMMAND
Los Angeles Air Force Station
P.O. Box 92960, Worldway Postal Center
Los Angeles, Calif. 90009

THE VIEWS AND CONCLUSIONS CONTAINED IN THIS DOCUMENT ARE THOSE OF THE
AUTHORS AND SHOULD NOT BE INTERPRETED AS NECESSARILY REPRESENTING THE
OFFICIAL POLICIES, EITHER EXPRESSED OR IMPLIED, OF THE DEFENSE ADVANCED
RESEARCH PROJECTS AGENCY OR THE U.S. GOVERNMENT

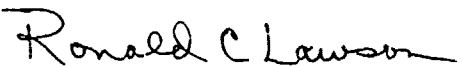
This research was supported by the Defense Advanced Research Projects Agency of the Department of Defense and was monitored by Space and Missile Systems Organization (SAMSO) under Contract No. F04701-75-C-0076.

Approved


S. Siegel, Director
Chemistry and Physics Laboratory

This technical report has been reviewed and is approved for publication. Publication of this report does not constitute Air Force approval of the report's findings or conclusions. It is published only for the exchange and stimulation of ideas.

FOR THE COMMANDER


Ronald C. Lawson
2nd Lt, United States Air Force
Office of Research Applications
Deputy for Technology

UNCLASSIFIED

SECURITY CLASSIFICATION OF THIS PAGE (When Data Entered)

REPORT DOCUMENTATION PAGE		READ INSTRUCTIONS BEFORE COMPLETING FORM
1. REPORT NUMBER SAMSO-TR-75-288	2. GOVT ACCESSION NO.	3. RECIPIENT'S CATALOG NUMBER
4. TITLE (and Subtitle) LINE-BY-LINE CALCULATIONS OF HOT-GAS SPECTRA INCLUDING HF AND HCl		5. TYPE OF REPORT & PERIOD COVERED Interim rept.
		5. PERFORMING ORG. REPORT NUMBER TR-0076(6970)-61
7. AUTHOR(s) Charles M./Randall		8. CONTRACT OR GRANT NUMBER(s) F04701-75-C-0076, 2 DAR-A 2943
9. PERFORMING ORGANIZATION NAME AND ADDRESS The Aerospace Corporation El Segundo, Calif. 90245		10. PROGRAM ELEMENT, PROJECT, TASK AREA & WORK UNIT NUMBERS 1567
11. CONTROLLING OFFICE NAME AND ADDRESS Defense Advanced Projects Agency 1400 Wilson Blvd. Arlington, Va. 22201		12. REPORT DATE 4 December 1975
		13. NUMBER OF PAGES 102
14. MONITORING AGENCY NAME & ADDRESS (if different from Controlling Office) Space and Missile Systems Organization Air Force Systems Command Los Angeles, Calif. 90009		15. SECURITY CLASS. (of this report) Unclassified
		15a. DECLASSIFICATION/DOWNGRADING SCHEDULE
16. DISTRIBUTION STATEMENT (of this Report) Approved for public release; distribution unlimited		
17. DISTRIBUTION STATEMENT (of the abstract entered in Block 20, if different from Report) D D C RECEIVED JAN 22 1976 REGISTRY D		
18. SUPPLEMENTARY NOTES		
19. KEY WORDS (Continue on reverse side if necessary and identify by block number) HCl HF Infrared Radiative Transfer Spectroscopy		
20. ABSTRACT (Continue on reverse side if necessary and identify by block number) Low- and medium-resolution (2 and 20 μm^{-1}) spectra are presented of hot nonuniform gas samples in the 2- to 5- μm spectral region based on line-by-line radiance computations. Two gas samples are considered. The first contains CO ₂ , CO, and H ₂ O as the active radiating species. The second contains HF and HCl as the active species. The radiation transmitted to the top of the atmosphere from these samples is also computed. The Air Force Cambridge Research Laboratories spectral line atlas was used to obtain line parameters for gases that are atmospheric constituents. The computation		

DD FORM 1473 (FACSIMILE)

UNCLASSIFIED
SECURITY CLASSIFICATION OF THIS PAGE (When Data Entered)

UNCLASSIFIED

SECURITY CLASSIFICATION OF THIS PAGE(When Data Entered)

19. KEY WORDS (Continued)

20. ABSTRACT (Continued)

from basic molecular constants of the required additional HCl and HF line parameters for the $v = 0-1, 1-2, 2-3, 3-4,$ and $0-2$ bands, including lines of importance in hot samples, is described in detail, and the resulting line parameters are listed. These computed line parameters agree well with available observations by several investigators at both low and high temperatures. As expected, the AFCRL atlas is found, by comparison with experimental spectra, to be quite adequate for modeling samples at terrestrial temperatures, but somewhat lacking in the lines required for complete modeling of samples at high temperatures.

R

UNCLASSIFIED

SECURITY CLASSIFICATION OF THIS PAGE(When Data Entered)

CONTENTS

SUMMARY	7
I. INTRODUCTION	9
II. AFCRL LINE ATLAS COMPARISON	11
A. Atmospheric CO ₂ Path (Test No. 1)	11
B. Atmospheric H ₂ O Path (Test No. 2)	14
C. Hot CO ₂ Paths (Tests No. 3 and 5)	14
D. Hot H ₂ O Path (Test No. 4)	18
E. Hot CO ₂ Path, 4.3- μ m Spectral Region (Test No. 6)	21
F. Nonisothermal Hot H ₂ O Path (Test No. 7)	21
III. HCl AND HF SPECTRAL LINE PARAMETERS	27
A. Basic Relations and Data	27
B. Computed Line Parameter Accuracy	42
C. HF Spectral Comparison	54
IV. HOT-GAS SPECTRA	59
REFERENCES	79
APPENDIX. LINE PARAMETERS FOR HCl ³⁵ , HCl ³⁷ , AND HF	A-1

ACCESSION for		
NTIS	White Section	<input checked="" type="checkbox"/>
DDC	Buff Section	<input type="checkbox"/>
UNANNOUNCED		<input type="checkbox"/>
JUSTIFICATION		
BY		
DISTRIBUTION/AVAILABILITY CODES		
Dist.	AVAIL. and/or SPECIAL	
A		

D D C

R E C E I V E D

JAN 22 1976

R E C E I V E D

D

TABLES

1.	Experimental Conditions for Comparison with Computed Spectra	12
2.	Dunham Coefficients for HF and HCl	29
3.	Parameters for Line Strength Computation	37
4.	Line-Width Parameters for HF and HCl	41
5.	Self-Broadening Parameter Derivation	43
6.	Comparison of Observed with Calculated 1-0 HCl ³⁷ Line Frequencies	45
7.	HF Line-Width Parameter Data	53
8.	Plume A Simulation Conditions	62
9.	Plume B Simulation Conditions	63

FIGURES

1.	Comparison of Computed and Experimental Low-Resolution CO ₂ Spectra	13
2.	Comparison of Computed and Experimental Medium Resolution CO ₂ Spectra	15
3.	Comparison of Computed and Experimental H ₂ O Spectra	16
4.	Comparison of Computed and Experimental Hot CO ₂ Spectrum	17
5.	Comparison of Computed and Observed Hot CO ₂ Transmittance	19
6.	Comparison of Computed and Observed Hot H ₂ O Transmittance	20
7.	Comparison of Computed and Observed Hot CO ₂ Spectra in the 4.3 μm Region	22
8.	Comparison of Experimental and Computed Characteristics of a Nonisothermal H ₂ O Sample	23
9.	Temperature Profile for Nonisothermal H ₂ O Computation	24
10.	Line-Width Parameter for HCl as a Function of m 	38
11.	Measured Line Widths of the R-Branch of the HCl Overtone for Several Temperatures	39
12.	Comparison of Computed and Experimental HCl Line Strengths for the 0-1 Band	46
13.	Comparison of Computed and Experimental HCl Line Strengths for the 0-2 Band	47
14.	Comparison of Computed and Experimental HCl Line Strengths for the 2-3 Band	48
15.	Comparison of Computed and Experimental HF Line Strengths for the 0-1 Band	50

FIGURES (Continued)

16.	Comparison of Computed and Experimental HF Line Strengths for the 0-2 Band	51
17.	Summary of HF Experimental Line-Width Parameter Data	52
18.	Comparison of the Computed HF Line Strengths of Goldman et al. at 1273 K with Values from the Present Study in the 2-3 Band	55
19.	Comparison of Experimental and Computed Characteristics of a Nonisothermal HF Sample	56
20.	Temperature Profile for Nonisothermal HF Computation	57
21.	Temperature and Species Concentrations for Plume A	60
22.	Temperature and Species Concentrations for Plume B	61
23.	Segment of the High-Resolution Plume A Radiance Spectrum	64
24.	Segment of the High-Resolution Plume B Radiance Spectrum in the HF Emission Region	65
25.	Computed Atmospheric Transmittance Between 2000 and 3200 cm^{-1}	66
26.	Computed Atmospheric Transmittance Between 3200 and 4100 cm^{-1}	67
27.	Computed Plume A Radiance Between 2000 and 3200 cm^{-1}	68
28.	Computed Plume A Radiance Between 3200 and 4100 cm^{-1}	69
29.	Apparent Plume A Radiance Between 2000 and 3200 cm^{-1}	70

FIGURES (Continued)

30.	Apparent Plume A Radiance Between 3200 and 4100 cm^{-1}	71
31.	Computed Plume B Radiance Between 2000 and 3200 cm^{-1}	72
32.	Computed Plume B Radiance Between 3200 and 4600 cm^{-1}	73
33.	Apparent Plume B Radiance Between 2000 and 3200 cm^{-1}	74
34.	Apparent Plume B Radiance Between 3200 and 4400 cm^{-1}	75
35.	Dependence of Apparent Transmittance on Source Spectrum Between 2000 and 3200 cm^{-1}	76
36.	Dependence of Apparent Transmittance on Source Spectrum Between 3200 and 4000 cm^{-1}	77

SUMMARY

Radiance spectra for two hot-gas samples have been computed using quasi-monochromatic calculation techniques and data from the Air Force Cambridge Research Laboratories (AFCRL) line atlas augmented with spectral data on HCl and HF. Apparent radiance at the top of the atmosphere has also been computed as has the effective average atmospheric transmittance, which depends on the source.

The adequacy of the AFCRL atlas for hot-gas modeling has been explored by comparison of experimental and computed spectra. The atlas was found to contain insufficient hot lines for accurate modeling of the wings of bands. Effort should be directed toward providing an adequate line atlas for hot-gas modeling.

The HF and HCl band line parameters include hot lines, but omit the H^2 isotopic species. Although the normal concentration of H^2 is only 0.0156 percent, the lines are strong enough to appear in the spectra. These lines should be added in the future. A more appropriate line-width parameter for high J values is also needed.

The Voigt line shape has not been used because of cost. Efficient approximations to the Voigt function should be obtained.

I. INTRODUCTION

High-resolution spectra of the radiation from a combustion-product source viewed through an atmospheric absorption path are required for several applications. An important example is the remote sensing of missiles or aircraft from their exhaust plume radiation. The measurement of these radiance spectra would require the use of research-laboratory-type instruments because the individual spectral lines are less than 0.1 cm^{-1} wide.* Because measurements are difficult in the field, recourse has been made to computations. If the pressure, temperature, and species concentrations are sufficiently well defined in the plume and atmosphere, and if the required spectral coefficients are available, the radiance can be computed by straightforward but tedious means. The procedures developed to make these computations at The Aerospace Corporation were described in an earlier report.¹

The spectral coefficients for the atmospheric gases were obtained from the Air Force Cambridge Research Laboratories (AFCRL) compilation.² Although this line compilation was never intended for plume modeling, it is the most comprehensive compilation available and, therefore, was used in the present study. The compilation has been revised since the comparisons presented in Ref. 1. In Section II, the revised version is compared with experimental measurements.

The spectra of sources that contain HCl and HF were investigated. The spectral coefficients for these gases were calculated from basic molecular parameters. These computations and a comparison of the results with experimental line parameters and experimental spectra are given in Section III. The calculated spectra are given in Section IV.

*In this report, the unit of frequency is wavenumber (cm^{-1}).

II. AFCRL LINE ATLAS COMPARISON

The AFCRL compilation of spectroscopic line parameters was originally designed to study the propagation of infrared radiation through the atmosphere. The atlas is adequate for these studies in the 2.7- μm regions, as the comparisons in Ref. 1 indicated. Since the publication of Ref. 1, revised editions of the line atlas have been received from AFCRL. In the revised version, the error in the 010-130 water band strength has been corrected, several additional water bands have been added in the 2.7- μm regions, and the CO_2 parameters have been significantly reworked throughout the infrared spectral region. Because of these changes, it was deemed beneficial to repeat the comparisons made in the previous study as well as to add some additional comparisons.

The AFCRL atlas, as revised, appears to be adequate for atmospheric paths. The comparisons indicate that, in spite of the hot bands that have been added, the line atlas is still only partially adequate for modeling gases with temperatures greater than 1000 K.

The conditions of the various test spectra are shown in Table 1. Most of the comparisons are in the 2.7- μm spectral region; the results of the comparisons are discussed below. Tests 1 through 4 were conducted for the same conditions as the tests in Ref. 1.

A. ATMOSPHERIC CO_2 PATH (TEST NO. 1)

Experimental CO_2 spectra characteristic of atmospheric paths have been obtained by Burch,³ and his sample 10 was chosen for comparison. The solid curve in Fig. 1 represents the experimental results and was obtained by differentiating a tabulated spectrum from Ref. 3; the dashed curve indicates the result obtained in the earlier study.¹ The results obtained with the most recent line atlas are shown as the broken curve. In general, the revised atlas gives results that approximate those of the old atlas and are in reasonable agreement with the experimental values. Both computed spectra

Table 1. Experimental Conditions for Comparison with Computed Spectra

Test Condition	Test No.						
	1	2	3	4	5	6	7
Total pressure, mb	101.3	963.6	2026.5	949.8	1010.6	13.47	893.3
Temperature, K	296.0	296.0	1146.0	1040.0	1200.0	1159.0	Inhomogeneous
Column density, 10 ²⁰ mol/cm ²							
H ₂ O	n	29.011	0	3.9689	0	0	5.3962
CO ₂	44.835	0	7.6349	0	0.47256	0.048823	0
Total path length, m	237.0	121.0	0.60	0.60	0.0775	0.60	0.60
Ref.	Sample 10, Ref. 3	Sample 39, Ref. 4	Fig. 6, Ref. 5	Fig. 47, Ref. 7	Test T4, Ref. 6	Test RCK2 ^a	Fig. B3, Ref. 5
Comparison	Figs. 1, 2	Fig. 3	Fig. 4	Fig. 6	Fig. 5	Fig. 7	Fig. 8

^aF. S. Simmons, Environmental Research Institute of Michigan, private communication, 9 August 1974.

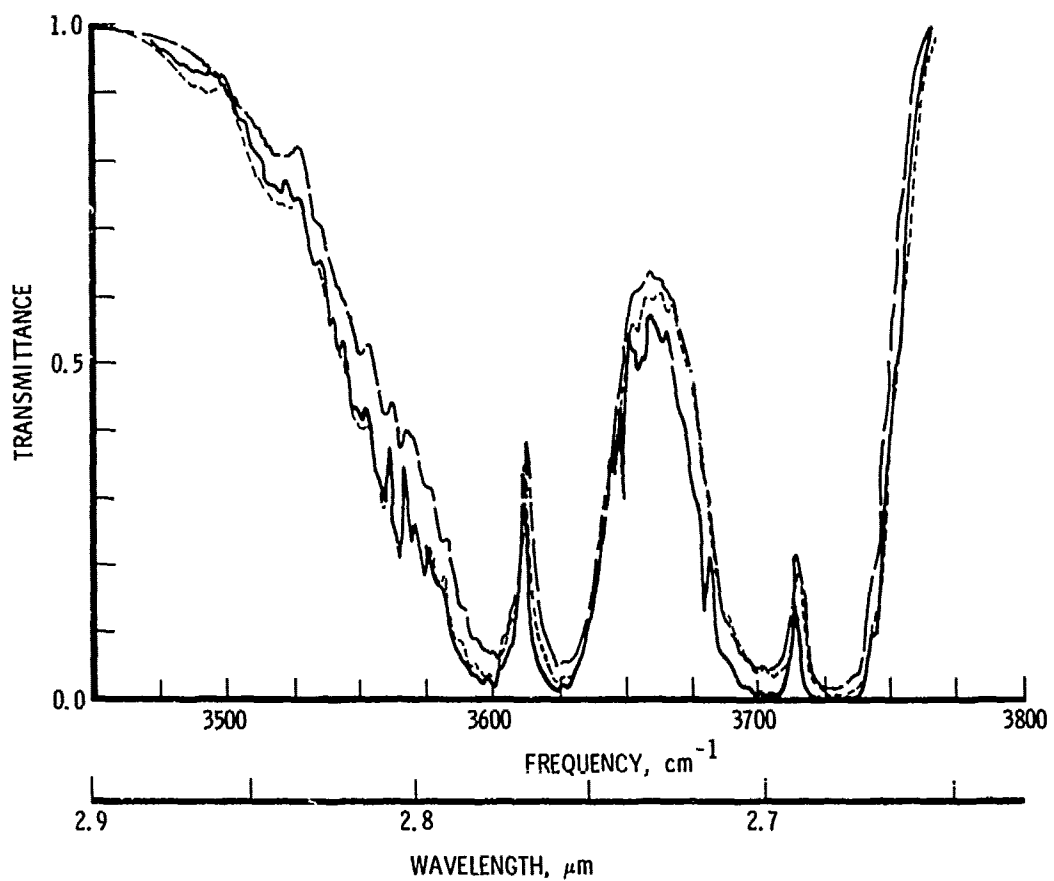


Figure 1. Comparison of Computed and Experimental Low-Resolution CO₂ Spectra. The solid curve is the experimental curve of Burch³ for a homogeneous path with conditions characteristic of an atmospheric path. The dashed curve was obtained from the AFCRL line atlas used by Randall.¹ The broken curve was computed for the same conditions, except that the revised AFCRL line atlas was used.

were obtained by convolving a 2.5-cm^{-1} full-width-at-half-maximum (FWHM) triangle with the high-resolution spectrum computed with the INHOM program and the line atlas indicated.

A higher-resolution spectrum for this same sample is shown in Fig. 2. The solid experimental curve was reproduced from Ref. 3 by procedures outlined by Randall.¹ The computed curves were obtained by convolving a 0.8-cm^{-1} -wide FWHM triangular function with the high-resolution spectrum. The dashed curve is based on the earlier line atlas. The results obtained with the revised atlas (broken curve) are shown only in the two regions where they differ most significantly from the earlier results. Although the differences are real, they are not large enough to be of great concern. The apparent closer agreement of the early atlas results with the experiment results is somewhat surprising.

B. ATMOSPHERIC H₂O PATH (TEST NO. 2)

The solid curve in Fig. 3 represents a portion of the experimental H₂O spectrum obtained by Burch, Gryvnak, and Patty⁴ and identified as sample 39. Computed curves were obtained by convolving a 0.5-cm^{-1} -wide FWHM triangle with the computed high-resolution spectrum. The strength of spectral lines of the 010-030 band at the positions indicated by the vertical bars in Fig. 3 were too large in the previous version of the line atlas. The dashed curve, which was obtained with the revised atlas, indicates that this problem has been corrected, and reasonably good agreement exists between the measured and experimental data.

C. HOT CO₂ PATHS (TESTS NO. 3 AND 5)

The solid curve in Fig. 4 represents the experimental radiance spectrum for Test No. 3, a hot, high-pressure sample of CO₂. The spectrum and experimental conditions were obtained from the work of Simmons, Yamada, and Arnold.⁵ The computational results were obtained by convolving a 5-cm^{-1} -wide FWHM triangular instrument function with the high-resolution spectrum. The dashed curve was obtained with the earlier AFCRL atlas. The broken

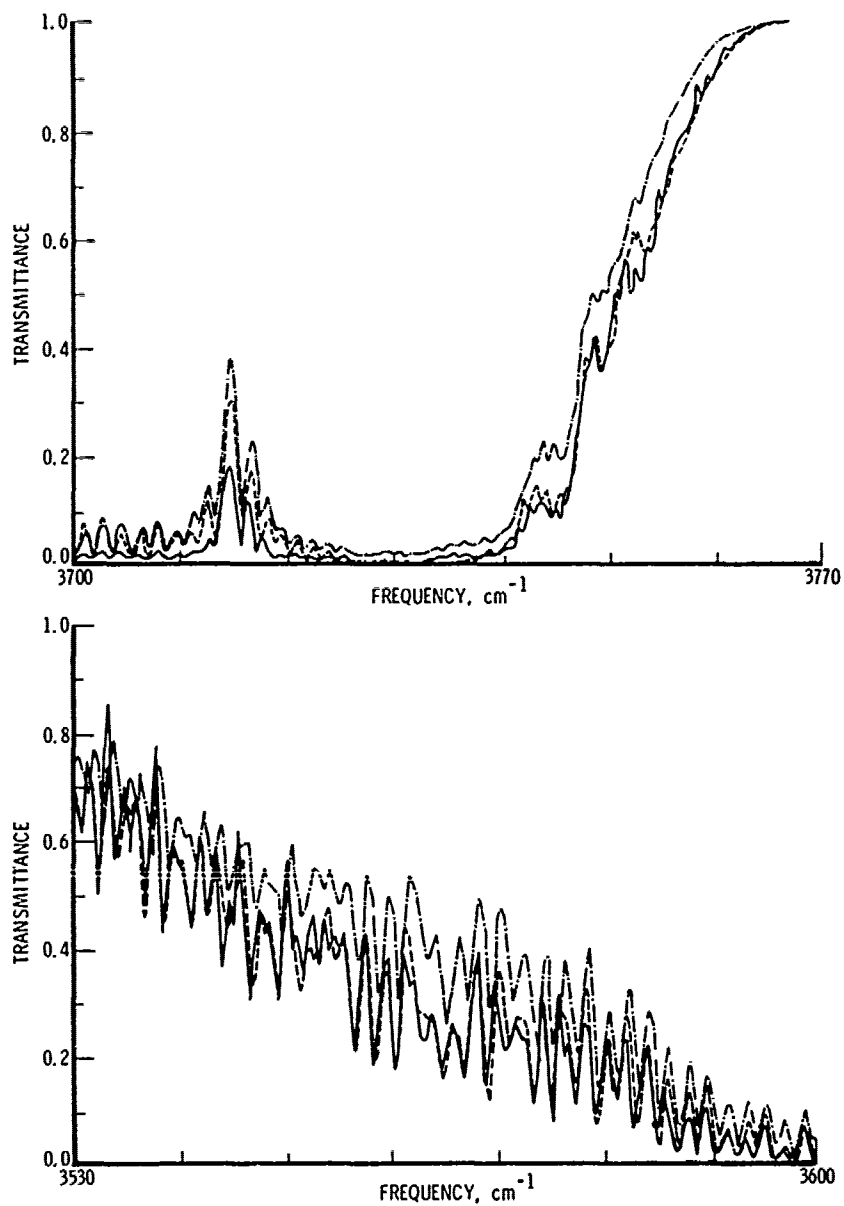


Figure 2. Comparison of Computed and Experimental Medium Resolution CO₂ Spectra. The same conditions apply as for Fig. 1, except at higher resolution. The spectral segments are those where the spectrum computed from the revised atlas (broken curve) deviates most significantly from the previously computed (dashed curve) and experimental results (solid curve)

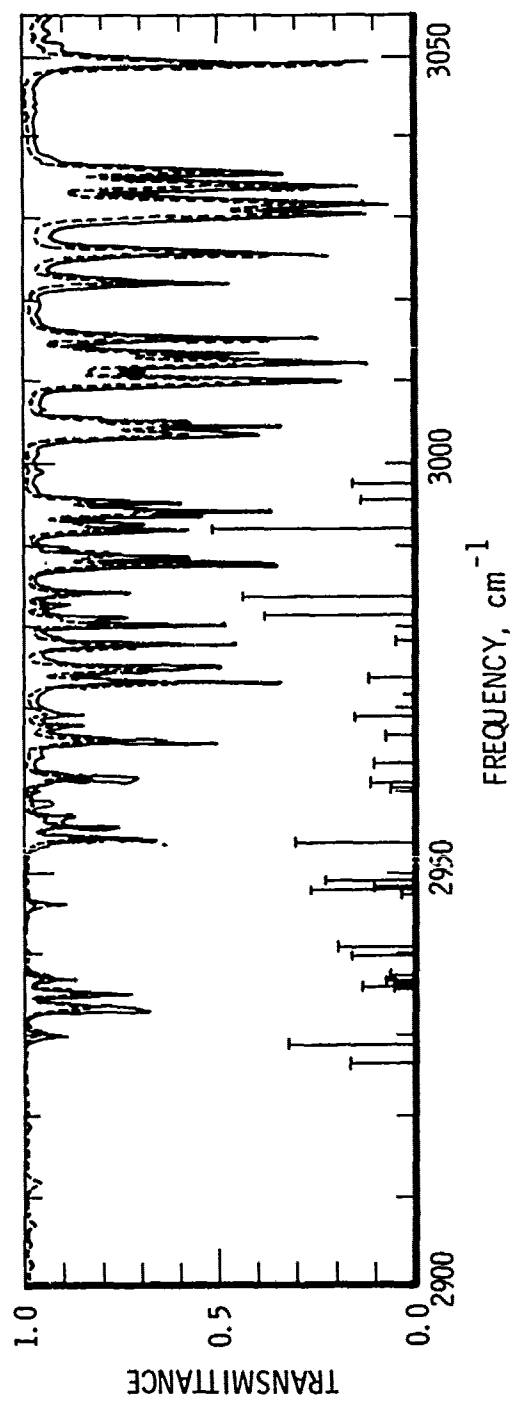


Figure 3. Comparison of Computed and Experimental H₂O Spectra. The solid curve is the spectrum obtained experimentally by Burch⁴ for homogeneous conditions representative of an atmospheric path. The dashed curve was computed from the revised line atlas. The vertical bars indicate the position of lines in the 010-030 band that had incorrect strengths in an earlier version of the atlas.

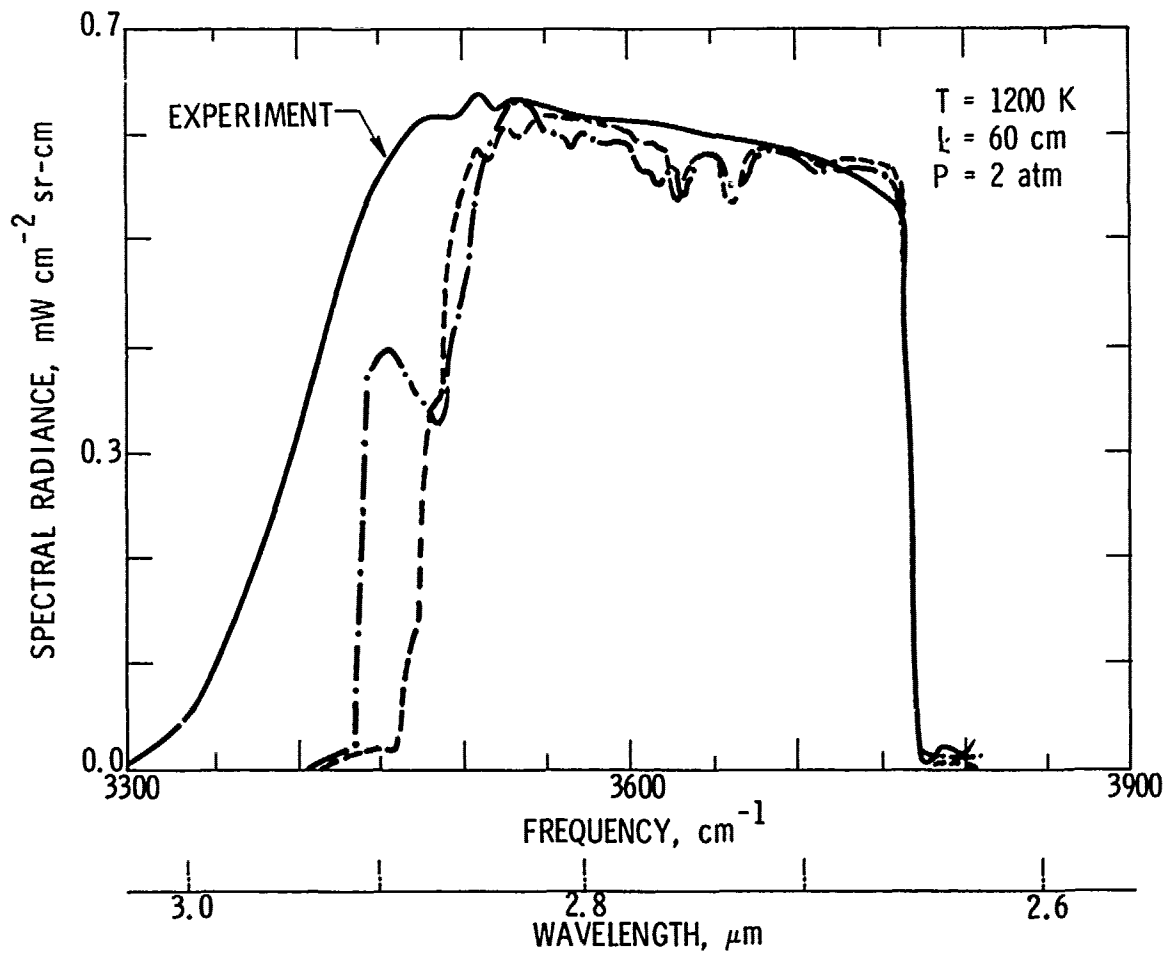


Figure 4. Comparison of Computed and Experimental Hot CO_2 Spectrum. The solid curve is the radiance observed by Simmons⁵ from a hot, high-pressure CO_2 sample. The dashed curve was computed for the same conditions but with the line atlas used in Ref. 1. The broken curve was computed from the revised line atlas.

curve is based on the revised atlas. In the wings of the band, many lines are clearly missing, even in the revised atlas. The deviation of the computed spectra from the experimental spectrum in the center of the band indicates that the line density or widths or both are not great enough in the atlas to make the sample optically thick, whereas, experimentally, the sample is optically thick.

A hot CO₂ sample (Test No. 5) for which the path is not optically thick in the 2.7- μ m band was studied experimentally by Burch and Gryvnak.⁶ Their result is shown as the solid curve in Fig. 5. The computational result (dashed curve) was obtained by convolving a 20-cm⁻¹-wide FWHM rectangular instrumental function with a high-resolution spectrum obtained with the INHOM program for the conditions listed and the revised line atlas. Again, the already noted deficiencies of the atlas in the wings of the CO₂ band and the inadequacies near the band center are apparent.

D. HOT H₂O PATH (TEST NO. 4)

The solid curve in Fig. 6 represents the experimental hot-water spectrum obtained from the work of Simmons, Arnold, and Smith,⁷ as described by Randall. The broken curve is the computed spectrum obtained by convolving a 7.5-cm⁻¹-wide FWHM triangular instrumental function with the high-resolution spectrum obtained with the revised line atlas. The error caused by the use of an incorrect 030-010 band intensity in the previous atlas has been corrected, and the differences between the computed and the experimental spectra are now in the expected direction. The computed transmittance is higher because of the lack of the hot lines in the atlas.

Comparison of Figs. 5 and 6 indicates that the AFCRL atlas is better capable of predicting the transmittance of hot H₂O than hot CO₂. Apparently, the percentage of water lines with significant strength at high temperatures included in the atlas is greater than the percentage of CO₂ lines.

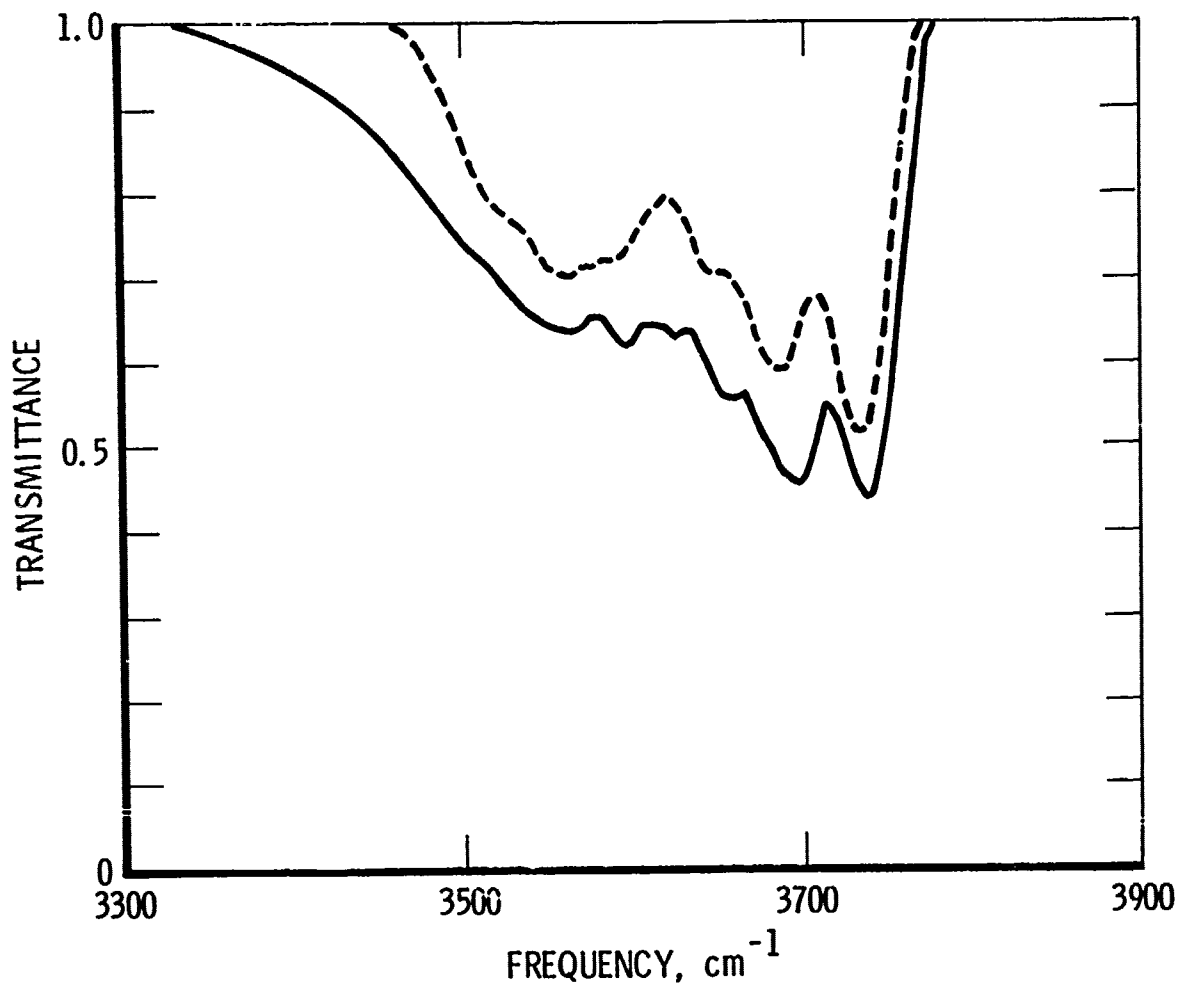


Figure 5. Comparison of Computed and Observed Hot CO₂ Transmittance. The solid curve is the spectrum observed by Burch.⁶ The dashed curve was computed from the revised line atlas.

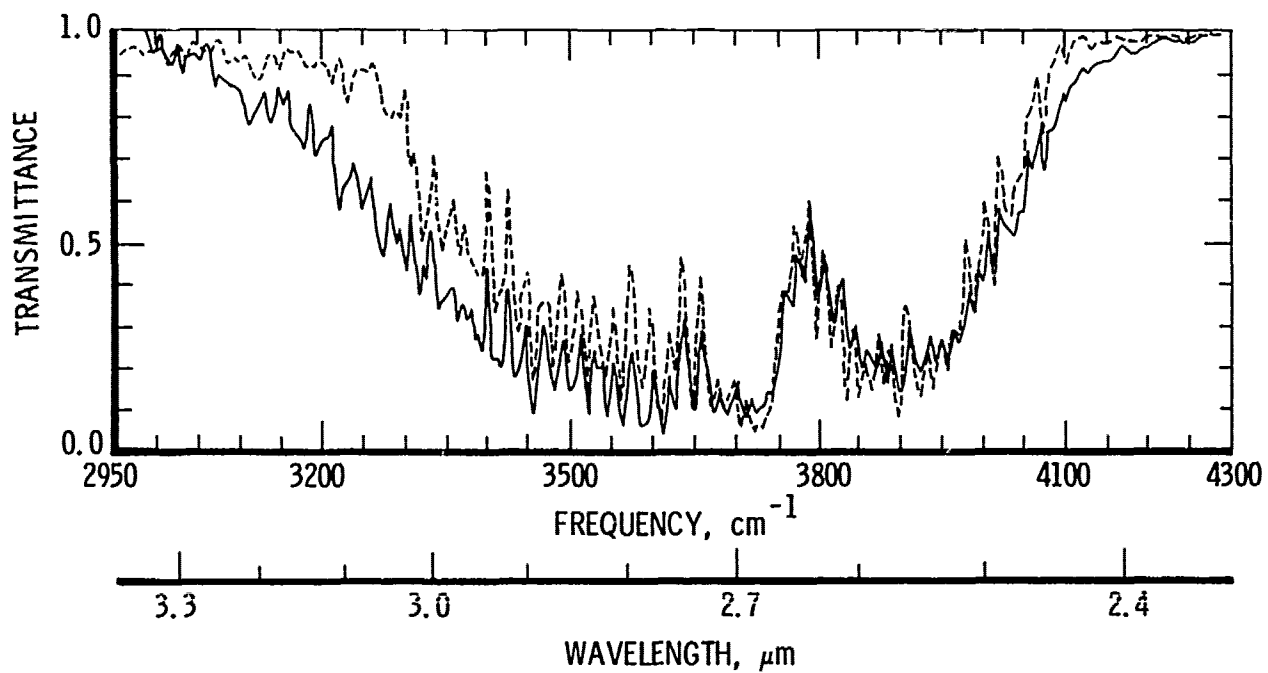


Figure 6. Comparison of Computed and Observed Hot H₂O Transmittance. The solid curve is the experimental curve of Simmons.⁷ The dashed curve was computed from the revised line atlas.

E. HOT CO₂ PATH, 4.3- μ m SPECTRAL REGION
(TEST NO. 6)

The solid experimental curve in Fig. 7 was obtained at the Environmental Research Institute of Michigan (ERIM).^{*} The dashed curve was obtained by convolving a 5-cm⁻¹-wide FWHM triangular instrument function with the high-resolution spectrum computed with the revised AFCRL atlas and with a pressure-broadened line shape. For the pressures involved in this experiment, a Voigt profile is more appropriate; however, because the Voigt profile is more complicated mathematically, and hence requires more computation time, only a portion of the spectrum was computed with the Voigt profile. The results are indicated by X's in Fig. 7. Although the use of a more correct profile improves the agreement with experiment, it is clear that the AFCRL atlas is inadequate for accurate plume modeling in this spectral region (4.3- μ m) also.

F. NONISOTHERMAL HOT H₂O PATH (TEST NO. 7)

The spectra for the only nonisothermal path considered in evaluating the AFCRL line atlas are shown in Fig. 8. The experimental spectra and gas sample conditions were obtained from the work of Simmons, Yamada, and Arnold.⁵ The temperature profile for the 60-cm-long optical path is shown in Fig. 9. The open data points denote the measured temperatures along the path, and the step-function curve is the profile used for the computations. Both radiance and transmittance spectra are shown in Fig. 8 inasmuch as the radiance depends on temperature through the blackbody function as well as through the line parameters. The theoretical spectra were obtained by convolving a 3.5-cm⁻¹-wide FWHM triangular instrument function with the high-resolution spectrum computed with the revised AFCRL atlas and are shown as smooth solid curves in Fig. 8.

*F. S. Simmons, private communication (9 August 1971).

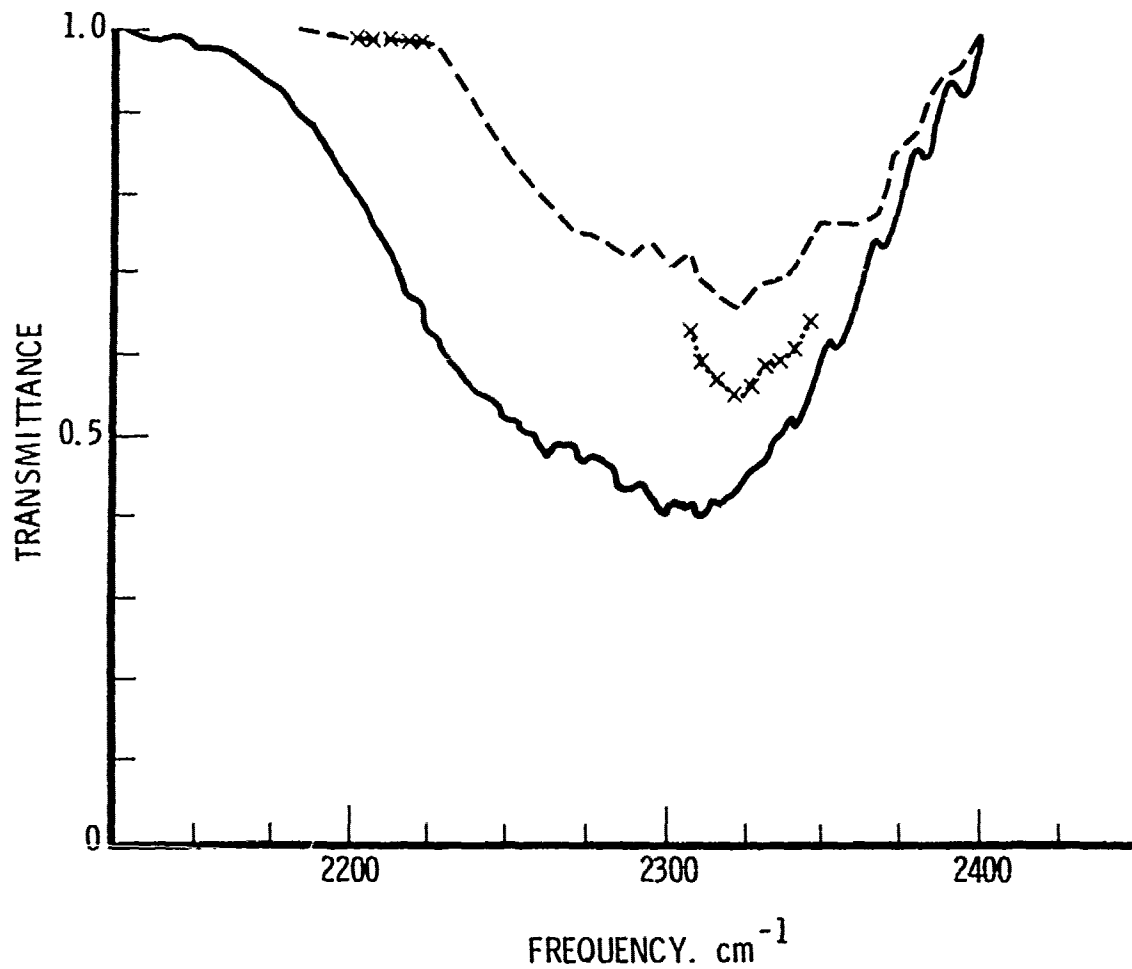


Figure 7. Comparison of Computed and Observed Hot CO₂ Spectra in the 4.3-μm Region. The solid curve was obtained experimentally at ERIM. The dashed curve was computed from the revised AFCRL atlas with use of a Lorentz line shape. The X-denoted curve was computed from the same line atlas with use of the more appropriate Voigt line shape.

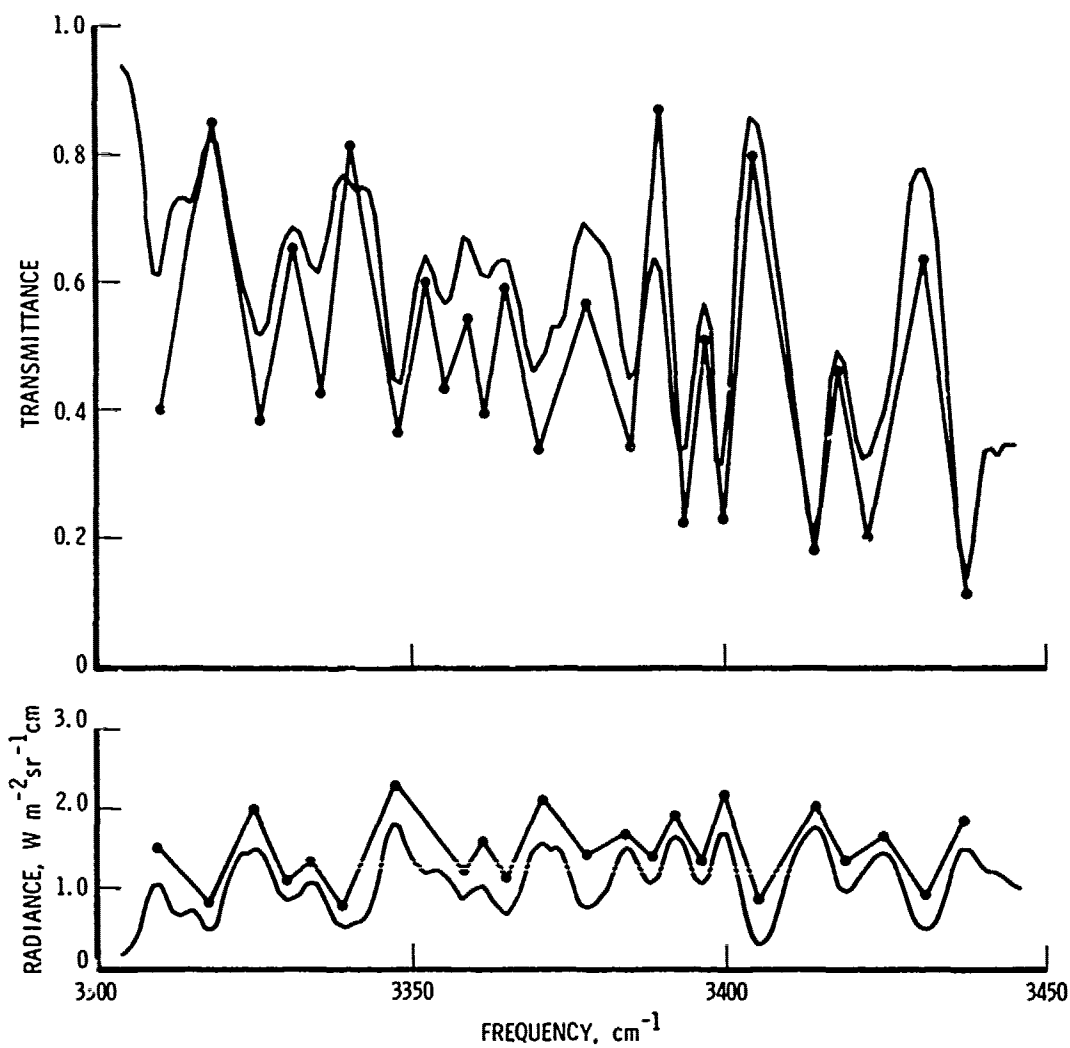


Figure 8. Comparison of Experimental and Computed Characteristics of a Nonisothermal H_2O Sample. The smooth curves are the computed transmittance and radiance for a path with the temperature profile shown in Fig. 9. The closed data points denote comparable experimental points from the work of Simmons.⁵

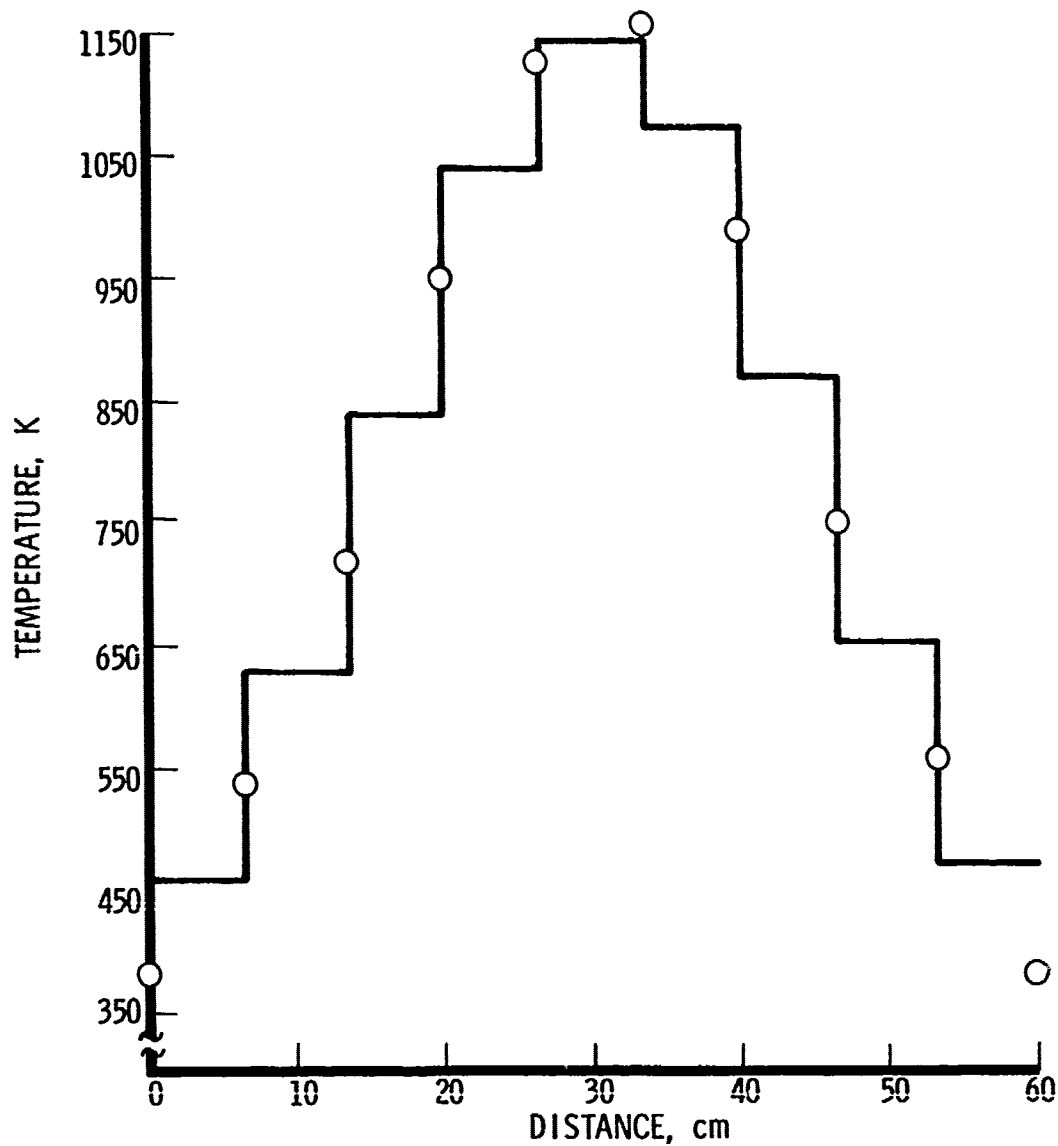


Figure 9. Temperature Profile for Nonisothermal H₂O Computation. The measured temperatures along the sample cell used to obtain the experimental points in Fig. 8 are shown (O). The horizontal line segments denote the temperature profile that was used to simulate the sample for computation.

The measured spectra in Ref. 5 are plotted such that reproduction on the scale of Fig. 8 would not produce a very meaningful comparison. Within the spectral region involved, there is a one-to-one correspondence between the spectral maxima and minima in the measured and computed spectra. These extreme values were obtained from Ref. 5 and are represented by the closed data points in Fig. 8. The solid curves connecting these points are included only as a visual convenience in following the curve and do not represent intermediate values actually measured.

In this spectral region, the agreement between experiment and computation is generally reasonable, although not perfect. In the transmittance plots, the tendency is for the computed results to underevaluate the absorption. This tendency is consistent with the results discussed in Section IID above.

III. HCl AND HF SPECTRAL LINE PARAMETERS

The computation of spectral radiance from plumes that contain HF and HCl requires that the line position ν , strength S , width a , and lower energy level E'' be available for all lines of interest. For hot plumes, the lines of interest include not only the transitions that involve the first few rotational levels of the $v = 1$ to $v = 0$ band, which have been studied extensively in the laboratory, but also transitions that involve higher vibrational and rotational levels. Fortunately, HF and HCl are simple diatomic molecules that have received extensive theoretical analysis. Procedures are therefore available for computing the energy levels, line positions, and strength from basic molecular constants. Pressure shifts of line positions are well documented for these gases, but were ignored in the present study because of the relatively low pressures that were used. The theoretical prediction of the pressure-broadening parameter is more difficult. In the present study, empirically determined line widths were used, where available, for low- J value lines. For other lines, a constant line width was used.

In this section, the basic equations used to determine the desired line parameters are presented together with the values of the molecular constants employed. Then, the accuracy of the various line parameters as determined by comparison with experimental data is discussed, and a computed HF spectrum is compared with an experimental spectrum.

A. BASIC RELATIONS AND DATA

1. ENERGY LEVELS

The energy levels or term values for a vibrating and rotating diatomic molecule have been studied extensively. The theory is well known and readily available.⁸ The effects of the interaction of vibration and rotation are accurately included in the Dunham formulation, in which the term value $\theta_{v,J}$ is

given in terms of a double series in the vibration quantum number v and the rotational quantum number J

$$\theta_{v,J} = \sum_{\ell=0}^{\ell=L} \sum_{m=0}^{m=M} Y_{\ell,m} (v + 1/2)^{\ell} J^m (J + 1)^m \quad (1)$$

The $Y_{\ell,m}$, known as Dunham coefficients, are usually determined by data-fitting techniques from the positions of spectral lines in carefully calibrated spectra. The values used in the present study for HF and HCl are given in Table 2. Sets of coefficients for HF and HCl³⁵ are available from the literature.^{9,10} A complete experimental analysis for HCl³⁷ was not found. Therefore, the HCl³⁷ set of coefficients was derived from the HCl³⁵ by means of the Dunham isotopic equation¹¹

$$Y_{\ell,m}^i = Y_{\ell,m} (\mu/\mu^i)^{q/2} \left[1 + \alpha_{\ell,m} (B_e/\omega_e)^2 (\mu - \mu^i)/\mu^i + \dots \right]$$

where μ is the reduced mass, and superscript i implies isotope and is not an exponent. The appropriate values of $q = \ell + 2m$ are given in Table 2. The $\alpha_{\ell,m}$ are of order unity. For HCl³⁵ and HCl³⁷

$$(B_e/\omega_e)^2 (\mu - \mu^i)/\mu^i \approx -2 \times 10^{-8}$$

Consequently, the terms involving this ratio were ignored. The value $(\mu/\mu^i)^{1/2} = 0.99924$ was used for deriving HCl³⁷ coefficients from HCl³⁵ values.

These term values include the zero-point energy of the oscillator. The approximation for the partition function in the present programs refers

Table 2. Dunham Coefficients for HF and HCl

Coefficient	HF, ^a cm ⁻¹	HCl ³⁵ , ^b cm ⁻¹	q	HCl ³⁷
				Value, cm ⁻¹
Y ₁₀	4138.73	2990.9463	1	2988.6732
Y ₂₀	-90.05	-52.81856	2	-52.73831
Y ₃₀	0.932	0.22437	3	0.22386
Y ₄₀	-1.42 × 10 ⁻²	-0.01218	4	-0.01214
Y ₅₀	-5.9 × 10 ⁻⁴		5	
Y ₀₁	20.9555	10.593416	2	10.577320
Y ₁₁	-0.7958	-0.307181	3	-0.306481
Y ₂₁	1.182 × 10 ⁻²	1.7724 × 10 ⁻³	4	1.7670 × 10 ⁻³
Y ₃₁	-3.11 × 10 ⁻⁴	-1.201 × 10 ⁻⁴	5	-1.196 × 10 ⁻⁴
Y ₄₁	-5.8 × 10 ⁻⁶		6	
Y ₀₂	-2.153 × 10 ⁻³	-5.31936 × 10 ⁻⁴	4	-5.30321 × 10 ⁻⁴
Y ₁₂	6.23 × 10 ⁻⁵	7.510 × 10 ⁻⁶	5	7.482 × 10 ⁻⁶
Y ₂₂	-2.06 × 10 ⁻⁶	-4.00 × 10 ⁻⁷	6	-3.98 × 10 ⁻⁷
Y ₀₃	1.68 × 10 ⁻⁷	1.74 × 10 ⁻⁸	6	1.732 × 10 ⁻⁸
Y ₁₃	-6.5 × 10 ⁻⁹	6.34 × 10 ⁻¹⁰	7	6.31 × 10 ⁻¹⁰
Y ₀₄	-1.0 × 10 ⁻¹¹	-9.93 × 10 ⁻¹³	8	-9.87 × 10 ⁻¹³

^aRef. 9^bRef. 10

all energy levels to the lowest vibrational level. Therefore, the lower energy level required from the line atlas for population computation is

$$E''_{v,J} = \theta_{v,J} - \theta_{0,0} \quad (2)$$

2. LINE POSITIONS

The frequency of a spectral line is given by the difference in term values for the upper and lower energy levels between which the transition occurs. The vibrational quantum number v can change by any integral value. Vibrational bands with $\Delta v \geq 2$ lie outside the spectral region of present interest and are excluded from the present study, except for the $v = 0$ to $v = 2$ band. Because of anharmonicities in the molecular vibration, the $\Delta v = 1$ bands are not all superimposed on each other. Four $\Delta v = 1$ bands with lower-level v numbers equal to 0, 1, 2, 3 are included in the present study. For the molecules of interest here, the rotational quantum number J can change by ± 1 . The R branch of the vibrational band corresponds to $\Delta J = +1$ when a photon is absorbed; the P branch corresponds to $\Delta J = -1$ when a photon is absorbed. The conventional notation is to indicate ΔJ by a letter and the J value of the lower state. With this notation, the frequencies of the lines may then be specified

$$\begin{aligned} \nu_{v',v'',J} &= \theta_{v',J+1} - \theta_{v'',J} && \text{(R Branch)} \\ \nu_{v',v'',J} &= \theta_{v',J-1} - \theta_{v'',J} && \text{(P Branch)} \end{aligned} \quad (3)$$

Note that there is no P(0) line.

3. LINE STRENGTHS

Line strengths are defined in several ways. For clarity, we first carefully define how line strengths are used in the computations performed

by the program described in Ref. 1. We then discuss how these line strengths are computed from basic molecular constants.

A homogeneous gas sample at temperature T with a single absorption line at ν_0 will have, for radiation at frequency ν , a transmittance

$$\tau = \exp [-S(T) W f(\nu, \nu_0)] \quad (4)$$

The line shape function is denoted by $f(\nu, \nu_0)$ and will have the unit of reciprocal frequency. For a pressure-broadened line of width a .

$$f(\nu, \nu_0) = a / \left\{ \pi \left[a^2 + (\nu - \nu_0)^2 \right] \right\} \quad (5)$$

W denotes a measure of the number of absorbing molecules present and is a column density with unit of molecules per unit area. The desired unit for the line strength is, then, frequency per unit column density. Specifically, for the present calculation, S has the unit $\text{cm}^{-1}/(\text{molecules cm}^{-2})$.

In the study of gases, where the ideal gas law is valid, the column density W can be related to the temperature T , pressure P , and length L of the sample by means of the Boltzmann constant k

$$W = PL/(kT) \quad (6)$$

If this is combined with Eq. (4)

$$\tau = \exp [-S(T) PL f(\nu, \nu_0)/(kT)] \quad (7)$$

The ratio $\sigma = S(T)/kT$ is also called the line strength by many authors; the usual unit is $\text{atm}^{-1} \text{cm}^{-2}$

The relationship between these two definitions of line strength is

$$\sigma = C_0 S/T$$

$$C_0 = 7.339083 \times 10^{21} \text{ molecules K cm}^{-3} \text{ atm}^{-1} \quad (8)$$

Except for comparison with experimental results, the line strength S is used exclusively in this report.

The line strength S depends on the fraction of the molecules in the energy level from which the transition begins and the matrix element $|R_{v'J'v''J''}|^2$ by the relations

$$S_{v'v''J'J''} = \frac{8\pi^3}{3hc} |R_{v'J'v''J''}|^2 |m| \nu_0 g(\nu_0, T) G_{v''J''} \quad (9)$$

$$m = \begin{cases} -J & \text{for P branch transitions} \\ J+1 & \text{for R branch transitions} \end{cases} \quad (10)$$

$$\nu_0 = \nu_{v', v'', J', J''}$$

$$g(\nu_0, T) = 1 - \exp(-hc\nu_0/kT) \quad (11)$$

$$G_{v'', J''} = \exp(-\theta_{v'', J''} hc/kT) / Z \quad (12)$$

$$Z = \sum_{v, J} (2J + 1) \exp(-\theta_{v, J} hc/kT) \quad (13)$$

where h is Planck's constant, 6.626196×10^{-27} erg sec; c is the velocity of light, 2.997925×10^{10} cm sec⁻¹; and k is Boltzmann's constant, 1.380622×10^{-16} erg K⁻¹.

The line strength S , as defined by Eq. (9), is a complicated function of temperature. Explicit account of all the various temperature variations would be time consuming. Therefore, for the spectral computations, the line strength S^0 computed at the standard temperature $T_0 = 296$ K by means of Eq. (9) is scaled to other temperatures by the relation

$$S = S^0 g(\nu, T) \exp \left[\frac{hcE''}{k} (1/T_0 - 1/T) \right] / z(T) \quad (14)$$

where $z(T)$ is the ratio of the partition function at T to the value of the partition function at T_0 . In order to avoid the summation implied by Eq. (13), z is approximated by the product of separate ratios for the vibrational and rotational partition functions

$$z(T) = Q_R(T) Q(T) = (T/T_0) [1 - \exp(-Y_{10}hc/kT)] \quad (15)$$

where Y_{10} is used as the vibrational frequency. No difference between HCl^{35} and HCl^{37} is recognized in calculating $z(T)$.

Except for the matrix elements, all the factors in Eq. (9) can be computed from the term values defined previously. Computation of the matrix elements requires computation of the integral of the radial wave functions $\phi(r)$ for the initial and final states with the electric dipole moment function $M(r)$

$$R_{\nu'v''J'J''} = \int_0^\infty \phi_{\nu'J'}(r) M(r) \phi_{\nu''J''}^*(r) dr \quad (16)$$

$M(r)$ is usually expanded in a power series about the equilibrium nuclear separation r_e

$$M(r) = \sum_j M_j (r - r_e)^j \quad (17)$$

Generally, the $\phi(r)$ functions can be generated most accurately by numerical solutions of the radial Schrödinger equation. The integral to obtain the dipole matrix elements is then also performed numerically. This procedure has been applied to several molecules, including HF and HCl³⁵, to obtain accurate line strengths.¹²⁻¹⁴ This approach requires a significant computational effort independent of the spectral computation of primary interest in the present study. Therefore, we elected to use the analytical approximations to Eq. (16) formulated by Herman and Wallis.¹⁵

In these analytical approximations for the matrix elements, the matrix element is written as a product of an anharmonic oscillator factor D and a correction factor F , which accounts for vibration-rotation interaction.

$$\left| R_{v', v'', J', J''} \right|^2 = \left| D_{v'' v'} \right|^2 F_{v'' v'}(J'') \quad (18)$$

Formulas for the $D_{v'' v'}$ are available¹⁵⁻¹⁷ in terms of the coefficient of the first power in the dipole moment function M_1 and spectroscopic constants defined in Eqs. (19)

$$\begin{aligned}
D_{01}' &= M_1 / (2\alpha)^{1/2} \\
D_{12} &= M_1 / \alpha^{1/2} \\
D_{23} &= M_1 / (2\alpha/3)^{1/2} \\
D_{34} &= M_1 / (\alpha/2)^{1/2} \\
D_{02}' &= M_1 b / (2\alpha)^{1/2}
\end{aligned} \tag{19}$$

where

$$\begin{aligned}
\alpha &= \omega_e / (2B_e r_e^2) \\
b &= -0.5Y^{1/2} (1 + \alpha_e / (3YB_e)) \\
Y &= 2B_e / \omega_e
\end{aligned} \tag{20}$$

The equilibrium spacing of the atoms is r_e ; the equilibrium rotation constant $B_e \approx Y_{01}$; the equilibrium vibration frequency $\omega_e \approx Y_{10}$; and the rate of change of B_e with v is $\alpha_e \approx -Y_{11}$.¹¹ Note that α and α_e are different quantities.

Formulas have also been computed for the vibration-rotation interaction correction terms F^{15-17}

$$\begin{aligned}
(F_{0,1})^{1/2} &= 1 - 2\theta Y m \left[1 + 7.5 b Y^{1/2} + 3Y - 2.5 b Y^{1/2} / \theta \right. \\
&\quad \left. + 0.75 b Y^{1/2} (m-1) / \theta + 0.375Y (m-1) / \theta \right] \\
(F_{1,2})^{1/2} &= 1 - 2\theta Y m \left[1 + 15 b Y^{1/2} + 6Y - 23 b Y^{1/2} / (4\theta) \right. \\
&\quad \left. + 0.75 b Y^{1/2} (m-1) / \theta + 0.375Y (m-2) / \theta \right]
\end{aligned} \tag{21}$$

(cont.)

$$\begin{aligned}
(F_{2,3})^{1/2} &= 1 - 2\theta Y m - 450 b Y^{3/2} m - 180 Y^2 m - 0.75 Y^2 m(m-3) \\
&\quad - 1.5 m^2 b Y^{3/2} + 39 m b Y^{3/2} / 2 \\
(F_{3,4})^{1/2} &= 1 - 2\theta Y m - 240 Y^2 m - 2990 m b Y^{3/2} / 4 \\
&\quad + 61 m b Y^{3/2} / 2 - 0.75 m^2 b Y^{3/2} - 0.75 Y^2 m(m-2) \\
(F_{0,2})^{1/2} &= 1 - 2 Y^{3/2} (m/b) \left[(1 - 0.75\theta + 0.5 b \theta / Y^{1/2}) - \theta Y m \right. \\
&\quad \left. + 0.5 (2 Y^{1/2} / b + 15/4) Y^{1/2} b (m+5) \right. \\
&\quad \left. + (3/16) Y^{1/2} b (2m-3) \right] \tag{21}
\end{aligned}$$

All the factors except $\theta = M_0/M_1 r_e$ have been previously defined.

The values used with Eqs. (9) through (13) and (18) through (21) to obtain the line strengths for the present work are given in Table 3. The data were taken from the references given in the table. The values of the dipole function expansion coefficients for HCl^{37} were obtained from the HCl^{35} values by multiplying by the square root of the 1:3 abundance ratio for Cl^{37} compared with Cl^{35} .

4. LINE WIDTHS

Pressure broadening of spectral lines results from collisions between molecules. The relative effectiveness of a collision in broadening a line depends on the molecules involved in the collision and on the energy state of the molecules. Collisions between molecules of the same type and in similar rotational states are the most effective collisions for the line broadening. The transition involved is much less important. These features are illustrated in Figs. 10 and 11.

The general similarity of the dependence of line width on the rotational quantum number factor $|m|$ [Eq. (10)] for a large variety of HCl transitions

Table 3. Parameters for Line Strength Computation

Quantity	Symbol	Unit	HF		HCl ³⁵		HCl ³⁷	
			Value	Ref.	Value	Ref.	Value	Ref.
Equilibrium nuclear separation	r_e	10^{-8} cm	0.916	16	1.2746	8	1.2746	8
Equilibrium rotation constant	B_e	cm^{-1}	20.9555	9	10.593416	10	10.577320	Table 2
Equilibrium vibration frequency	ω_e	cm^{-1}	4138.73	9	2990.9463	10	2988.6732	Table 2
Rate of change of B with vibration	α_e	cm^{-1}	0.7958	9	0.307181	10	0.306481	Table 2
First coefficient in dipole function expansion	M_0	10^{-18} esu cm	1.819	26	1.0935	14	0.63133	Text
Second coefficient in dipole function expansion	M_1	10^{-10} esu	1.5	26	0.947	14	0.546	Text
Partition function at	Z		4.947×10^{-4}	Eq. (12)	2.2369×10^{-2}	Eq. (12)	2.2523×10^{-2}	Eq. (12)

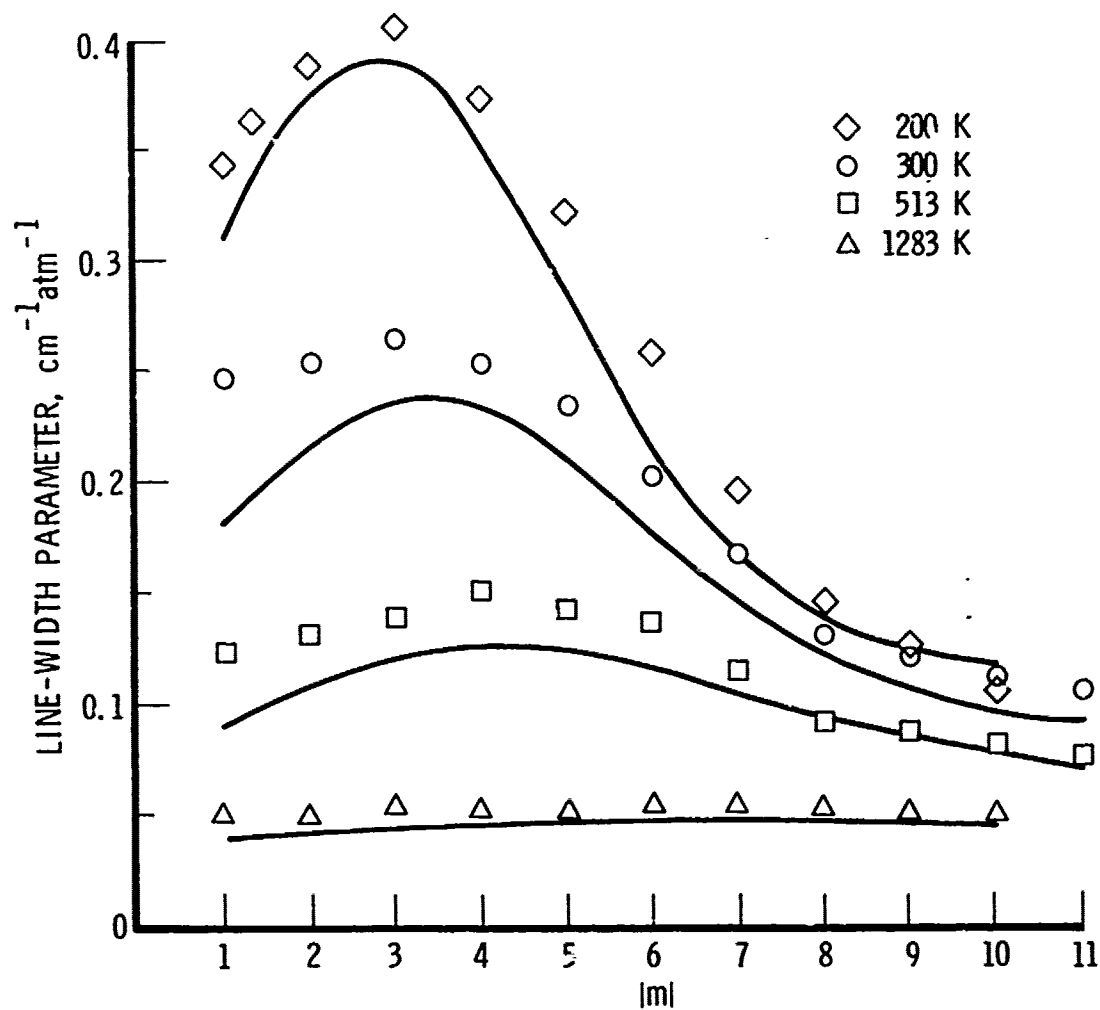


Figure 11. Measured Line Widths of the R Branch of the HCl Overtone for Several Temperatures. The solid curves were calculated from the Anderson theory for resonant dipoles with temperature-dependent hard cores. Taken from Goldring and Benesch.²⁰

is illustrated in Fig. 10. The open and closed triangles and circles from the work of Benedict et al.¹⁸ represent the P and R branches of the 1-0 band of HCl³⁵ and HCl³⁷; the crosses represent the 4-0 band of HCl as reported by Benedict et al. from the work of Lindholm;¹⁹ the X's represent the 2-0 band of HCl as measured by Goldring and Benesch;²⁰ and the ellipses represent the P branch of the 1-0 band as measured by Babrov, Ameer, and Benesch.²¹ These are all self-broadening coefficients, i. e., coefficients for collisions of HCl with HCl. The solid curve joins the values selected for HCl in the present study. N₂ is a much less efficient broadening agent, as is noted by the data taken from the work of Benedict et al.¹⁸ for nitrogen broadening and denoted by open squares in Fig. 10.

The shape of the relationship between $|m|$ and broadening is temperature dependent, as is shown in Fig. 11, which was taken from Ref. 20. The broadening parameters for the R branch of the HCl fundamental are plotted in the figure as a function of $|m|$ for a variety of temperatures. The flattening of the curve as the temperature is increased may be easily understood in a qualitative sense. The most effective broadening collisions are between molecules in similar J states. At low temperatures, most of the molecules are in a low J state. Thus, the probability of collisions with a molecule in a similar J state is high. As the temperature increases, the distribution in J states becomes less peaked, and any given collision is less likely to be with a molecule in a similar J state.

The qualitative features illustrated in Fig. 10 guided the empirical assignment of line width parameters in the present study. The variation in the relative shape of the broadening parameter curve with temperature was not included because of complications in using this information in actual spectral calculations.

The line width parameters assigned for HCl and HF taken from Benedict et al.¹⁸ and Smith²² are given in Table 4. Line widths for $|m|$ values greater than those for which data are available were assigned the constant values shown in the table.

Table 4. Line-Width Parameters for HF and HCl

$ m $	HCl, ^a $\text{cm}^{-1} \text{atm}^{-1}$	HF, ^b $\text{cm}^{-1} \text{atm}^{-1}$
1	0.218	0.56
2	0.223	0.67
3	0.249	0.63
4	0.246	0.50
5	0.227	0.33
6	0.186	0.24
7	0.153	0.15
8	0.127	0.10
9	0.106	0.10
10	0.0896	0.10
11	0.0842	0.10
12	0.0834	0.10
13	0.066	0.10
>13	0.06	0.10

^aRef. 18

^bRef. 22

The spectral computation program¹ computes a composite line width a appropriate for a particular path segment. The computation is based on the partial pressures P_i of the various gases present in that segment and the line width parameter a_0

$$a = a_0 (T_0/T)^{1/2} \sum_i \eta_i P_i$$

The coefficients η_i are the ratios of the foreign-gas broadening to self-broadening coefficients for the various gases included in the program. The values of η_i were estimated from the work of Babrov, Ameer, and Benesch²¹ for HCl (Table 5). The values of η used for CO₂ and CO are the average ratios shown in Table 5. All gases other than the halide, CO, and CO₂ are assumed to be air. For air, $\eta = 0.279$ is obtained by taking a weighted average of the values for N₂ and O₂ in Table 5. Based on the empirical results of Shaw and Lovell,²³ the η coefficients derived for HCl were also used for HF.

B. COMPUTED LINE PARAMETER ACCURACY

The calculated HF and HCl spectra in this report are based on a set of spectral line parameters that were computed from data presented in the preceding section for all J values up to 50 for the 0-1, 1-2, 2-3, 3-4, and 0-2 bands of HCl³⁵, HCl³⁷, and HF. This set includes all lines of these bands for which a 0.5-m path through a 1-atm 3000-K sample of the gas would have a peak absorptance of 0.01 or more. With an arbitrary cutoff in J, a number of weaker lines are also included. A more rational selection criterion was applied in selecting the line parameters given in the Appendix. There, the parameters are given only for lines that yield an absorptance greater than 10^{-2} for a 1-m path through a 3000-K sample of the gas at 1-atm pressure.

Table 5. Self-Broadening Parameter Derivation

Line	HCl-HCl Line- Width Parameter $\text{cm}^{-1} \text{atm}^{-1}$	Ratio Foreign-gas Broadening/ HCl Broadening			
		CO_2	CO	N_2	O_2
P1	0.207	0.807	0.565	0.447	0.341
P2	0.233	0.600	0.429	0.365	0.218
P3	0.231	0.445	0.415	0.313	0.166
P4	0.227	0.392	0.368	0.283	0.147
P5	0.207	0.351	0.327	0.286	0.142
P6	0.171	0.385	0.348	0.254	0.158
P7	0.145	0.346	0.394	0.250	0.150
P8	0.124	0.380	0.280	0.215	0.173
Average value		0.463	0.391	0.302	0.187

The accuracy of line positions is about 0.04 cm^{-1} for HF and about 0.005 cm^{-1} for the HCl positions. The lower energy levels are determined with similar precision. The line strengths are accurate to within 20 percent for low v and J values. The uncertainty increases for higher J and v values. The pressure-broadening coefficients are within 50 percent for low temperature and $m \leq 10$; they are less accurate for other conditions. These statements of accuracy are demonstrated in the next several paragraphs by comparison of calculated line parameters with experimental values.

The line frequencies of HCl are the most accurate quantities. The Dunham parameters from Ref. 10 were obtained for HCl^{35} . Our calculated HCl^{35} line positions agree, to within 0.001 cm^{-1} , with the calculated values

of Rank et al., which, in turn, agree with the observed frequencies to within about 0.004 cm^{-1} . An independent check on both the HCl^{35} Dunham coefficients and the conversion to HCl^{37} coefficients is provided by the data in Table 6, where observed 1-0 band HCl^{37} line frequencies²⁴ are compared with the values calculated with the parameters given in Table 2. The differences are somewhat larger than with the HCl^{35} observations, as would be expected, but the accuracy in this band is still better than 0.01 cm^{-1} .

The accuracy of the HF observations of Mann et al.⁹ is lower than that of the HCl observations. Consequently, the Dunham coefficients are given with lower accuracy. Comparison of computed and calculated values indicates an accuracy of about 0.04 cm^{-1} .

The lower energy levels are based on the same data as the line frequencies and hence should have a comparable accuracy. This is several orders of magnitude more accuracy than is required for scaling the very much less precise line strengths with temperature.

There are only a limited number of experimental line strength values available for HCl, and these are restricted to the lower rotational states. In Fig. 12, the calculated values for the 0-1 band (solid curve) are compared with the experimental values of Babrov, Ameer, and Benesch²¹ (squares) and the experimental values of Benedict et al.¹⁸ (circles). In Fig. 13, the calculated values for the 0-2 band (solid curve) are compared with the experimental values of Benedict et al.²⁵ These two sets of experimental data differ from each other and from the calculated values by 10 to 20 percent. This is the uncertainty we associate with the line strength for these bands. For higher vibrational states, the uncertainty in band strength can be expected to be somewhat larger.

Line strength at high temperature can be expected to have a decreased accuracy because of the scaling approximations, Eqs. (14) and (15), as well as the extrapolation of the basic theory to higher excitation levels. In Fig. 14, line strengths for the $v = 2$ to $v = 3$ band of HCl are compared with

Table 6. Comparison of Observed with Calculated 1-0 HCl³⁷ Line Frequencies

J	Observed, cm ⁻¹	Calculated, cm ⁻¹	10 ³ (Obs-Calc), cm ⁻¹	Observed, cm ⁻¹	Calculated, cm ⁻¹	10 ³ (Obs-Calc), cm ⁻¹
0	2904.1128	0.104	8.8	2863.0243	0.017	7.3
1	2923.7307	0.725	5.7	2841.5865	0.576	10.5
2	2942.7245	0.715	9.5	2819.5588	0.553	5.8
3	2961.0701	0.061	9.1	2796.9709	0.963	7.9
4	2978.7538	0.751	2.8	2773.8239	0.817	6.9
5	2995.7814	0.775	6.4	2750.1512	0.130	1.2
6	3012.1257	0.120	5.7	2725.9214	0.913	8.4
7	3027.7729	0.774	- 1.1	2701.1922	0.181	11.2
8	3042.7253	0.728	- 2.7	2675.9614	0.946	15.4
9	3056.9689	0.970	- 1.1	2650.2275	0.223	4.5
10	3070.4910	0.490	1.0	2624.0297	0.025	4.7
11	3083.2725	0.276	- 3.5	2597.3762	0.365	11.2
12	3095.3294	0.320	9.4	2570.2681	0.257	11.1
13	3106.6125	0.611	1.5	2542.7250	0.715	10.0
14	3117.1451	0.140	5.1	2514.7532	0.751	2.2
15	3126.8894	0.898	- 8.6	2486.3687	0.379	-10.3
16	3135.8750	0.875	0	2457.5929	0.613	-20.1
17	3144.0776	0.063	14.6	2428.4691	0.467	2.1
18	3151.4700	0.454	16.0	2398.9617	0.952	9.7
19	3158.0404	0.038	2.4			
20	3163.8152	0.809	6.2			
21	3168.7859	0.758	27.9			
22	3172.9152	0.878	37.2			

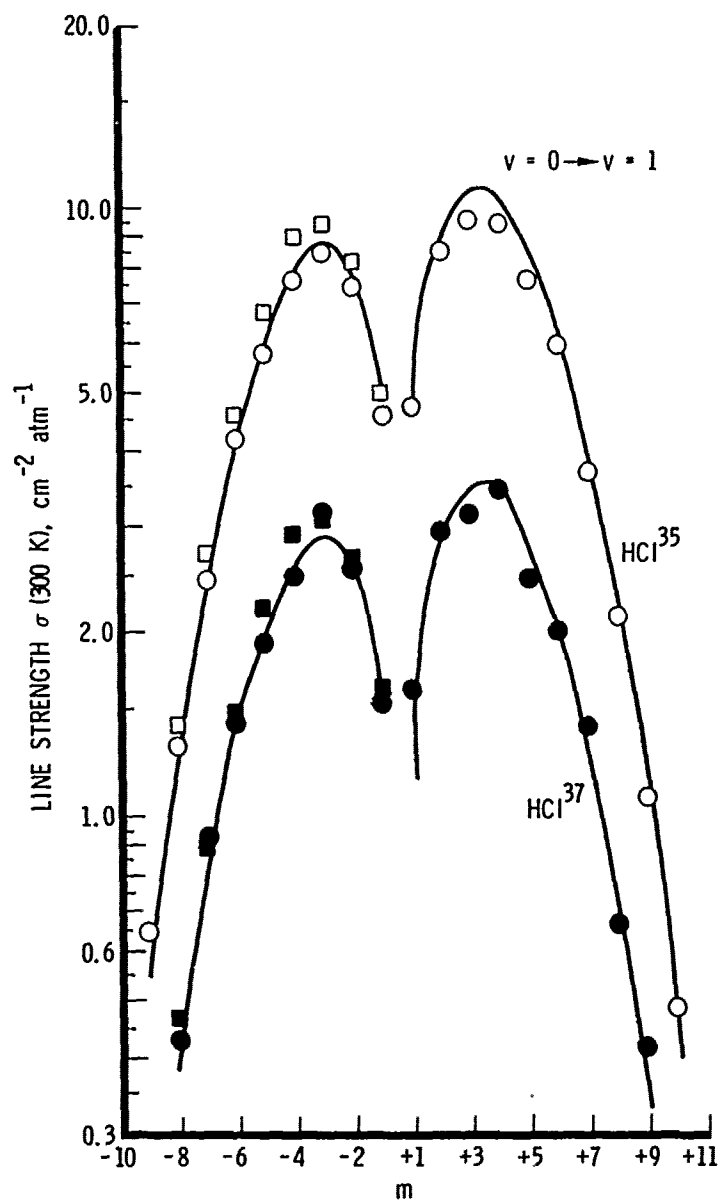


Figure 12. Comparison of Computed and Experimental HCl Line Strengths for the 0-1 Band. The values obtained in the present study are connected by a solid curve. Open symbols denote experimental HCl³⁵ values; closed symbols represent HCl³⁷ values. Values denoted by circles are from Ref. 18, those denoted by squares are from Ref. 21.

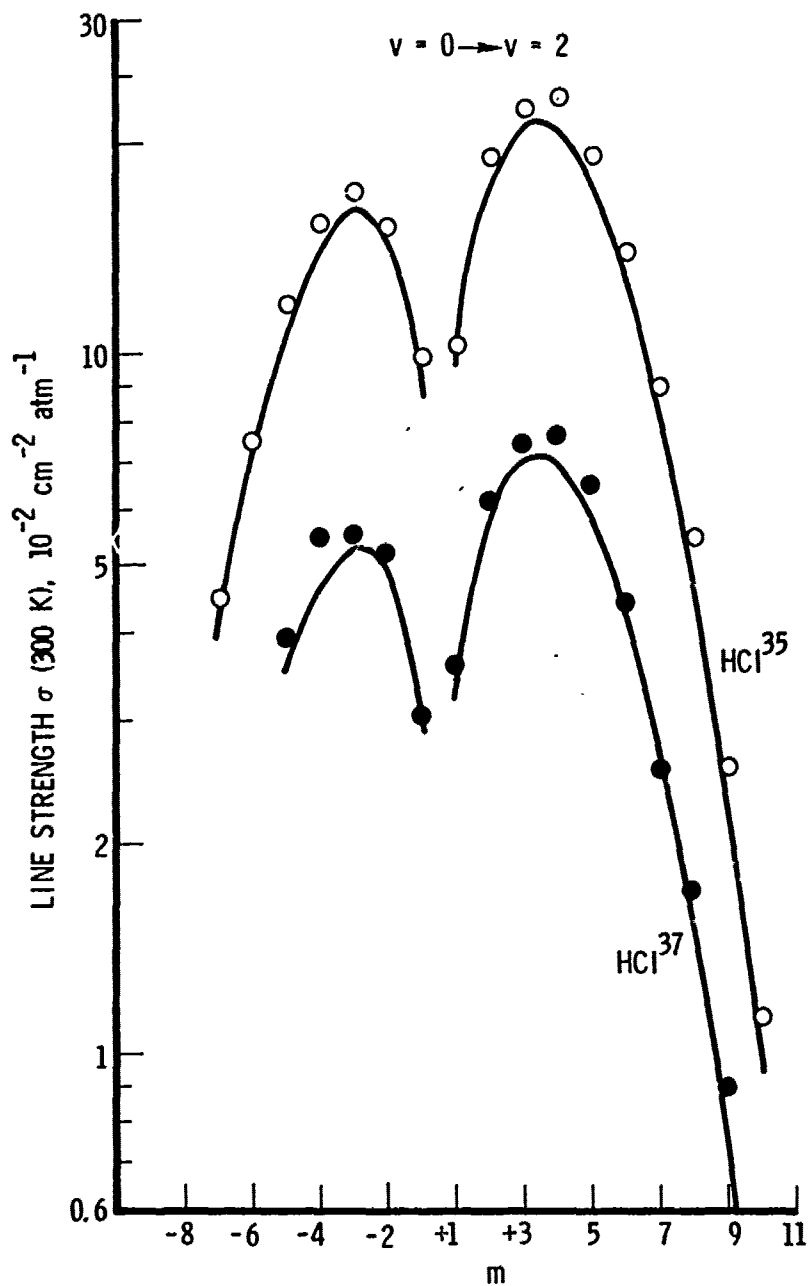


Figure 13. Comparison of Computed and Experimental HCl Line Strengths for the 0-2 Band. The values obtained in the present study are connected by a solid curve. Open symbols denote HCl³⁵ experimental values; closed symbols denote HCl³⁷ values. All experimental values are from Ref. 25.

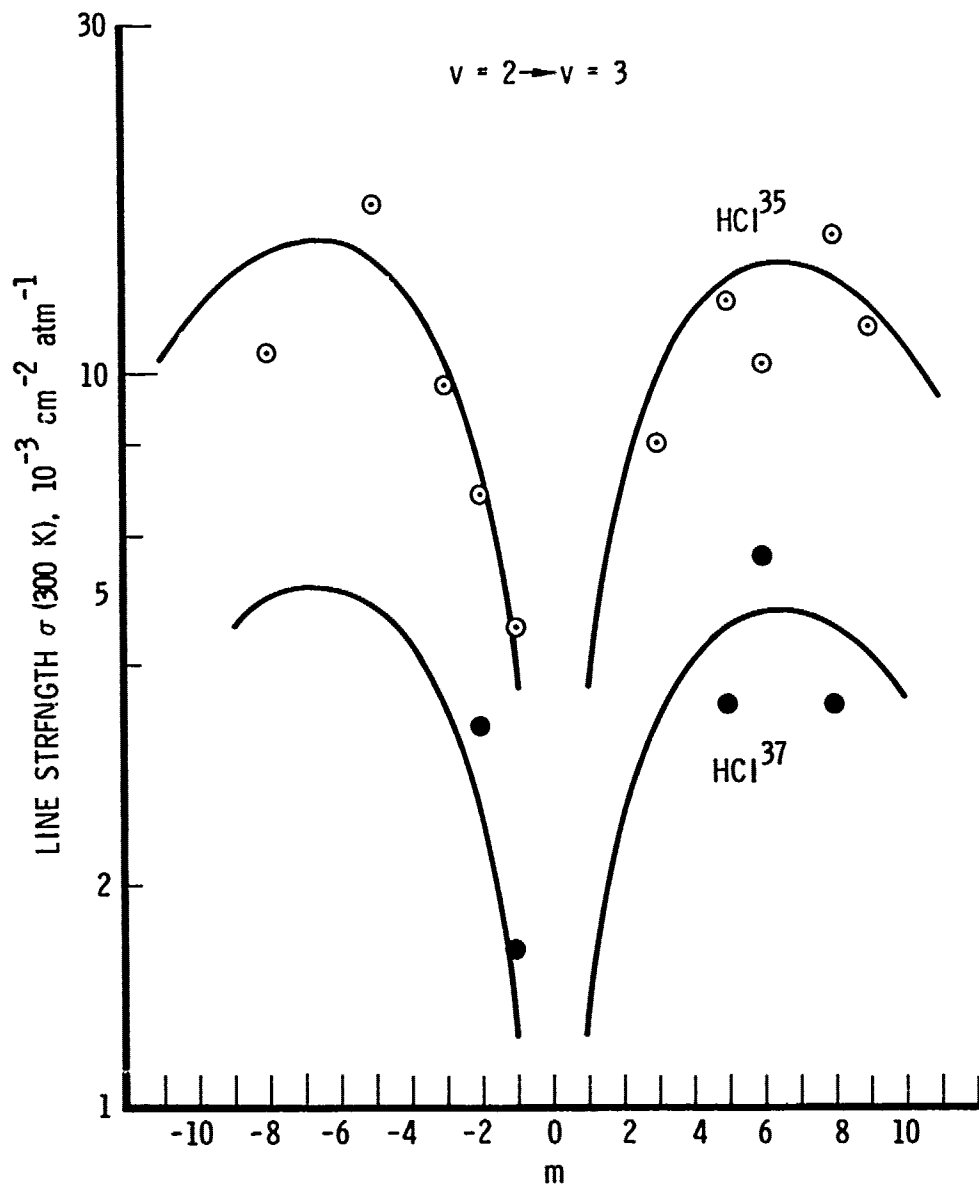


Figure 14. Comparison of Computed and Experimental HCl Line Strengths for the 2-3 Band. The values obtained in the present study, scaled to 1200 K as discussed in the text and reduced to units of σ at 300 K, are connected by a solid curve. The experimental values in these same units reported in Ref. 25 for HCl^{35} (O) and HCl^{37} (●) are also shown.

the values obtained by Benedict et al.²⁵ at 1200 K and values scaled from the 296 K line strengths by use of Eqs. (14) and (15). Although the agreement is poorer than for the lower temperatures and vibrational quantum numbers, all of the experimental points are still within 50 percent of the calculated values.

In Fig. 15, the computed line strengths for the 0-1 band of HF are compared with experimental measurements of Lovell and Herget,²⁶ Shaw and Lovell,²³ and Kuipers.²⁷ The comparisons are made for a temperature of 390 K because most measurements are made in this temperature range in order to avoid dimerization of the HF. The computed line strengths for 296 K have been scaled to 390 K by means of Eqs. (14) and (15). Except for the P(8) and P(9) lines, the strengths all agree with each other and with the computed values to within 20 percent.

In Fig. 16, the computed line strengths for the 0-2 band of HF are compared with the observations of Meredith.²⁸ In view of the good agreement in Fig. 15, the rather consistent deviation of the measured and computed values for the low $|m|$ values is puzzling, and we are unable to explain it. However, the measured and calculated values are still within 30 percent of each other.

Data on line widths for HCl have been summarized in Fig. 10. The line-broadening parameters for low temperatures and values of $m \leq 13$ are probably within 20 percent of the true values. For higher rotational values and higher temperatures, greater deviations are expected between the parameters used for calculations of spectra and the true values.

HF line-width parameters are usually measured at 390 K or greater in order to avoid problems with HF dimers. The extreme values observed at this temperature in five different studies by Smith,²² Shaw and Lovell,²³ Lovell and Herget,²⁶ Kuiper,²⁷ and Meredith²⁸ are indicated in Fig. 17 by vertical bars and listed in Table 7. The values obtained from the 302 K data of Smith²² and used in the line-parameter compilations have been scaled

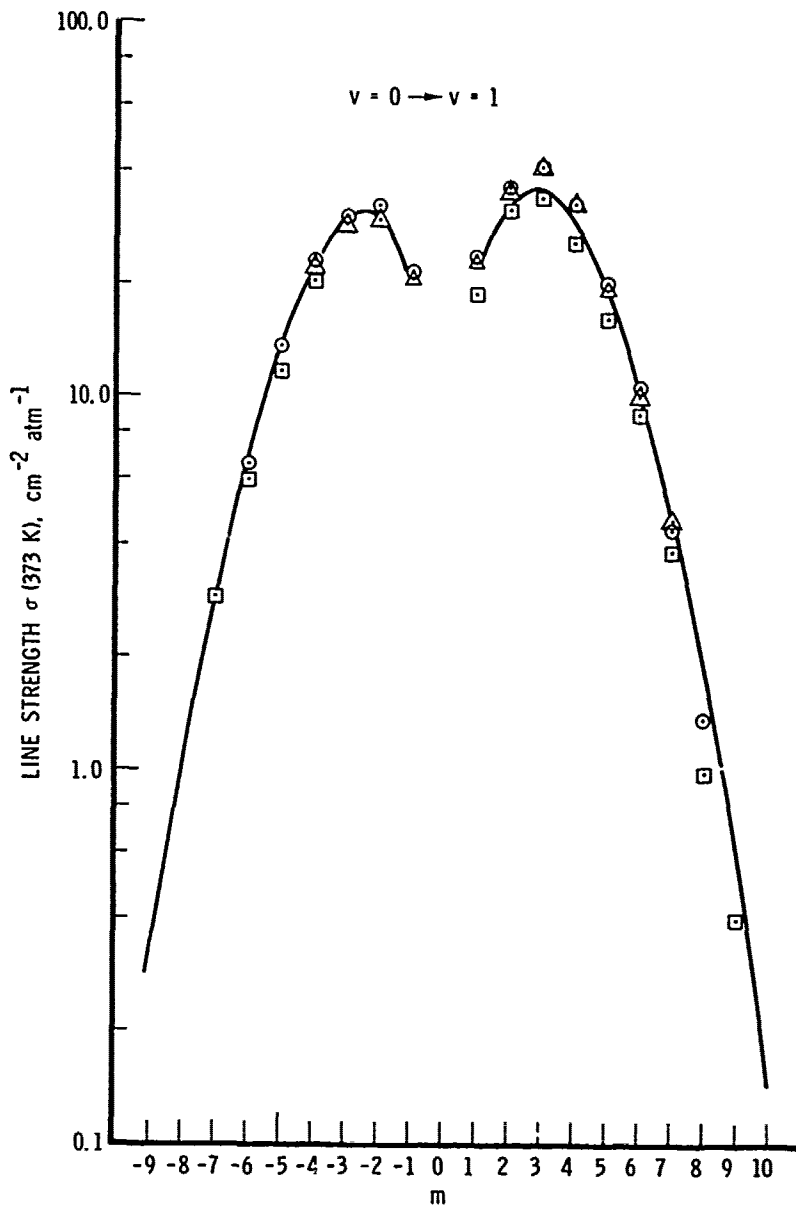


Figure 15. Comparison of Computed and Experimental HF Line Strengths for the 0-1 Band. The values obtained in the present study are connected by a solid curve. Experimental values are denoted by \square , Kuipers;²⁷ Δ ,²⁶ Shaw and Lovell;²³ O , Lovell and Herget.

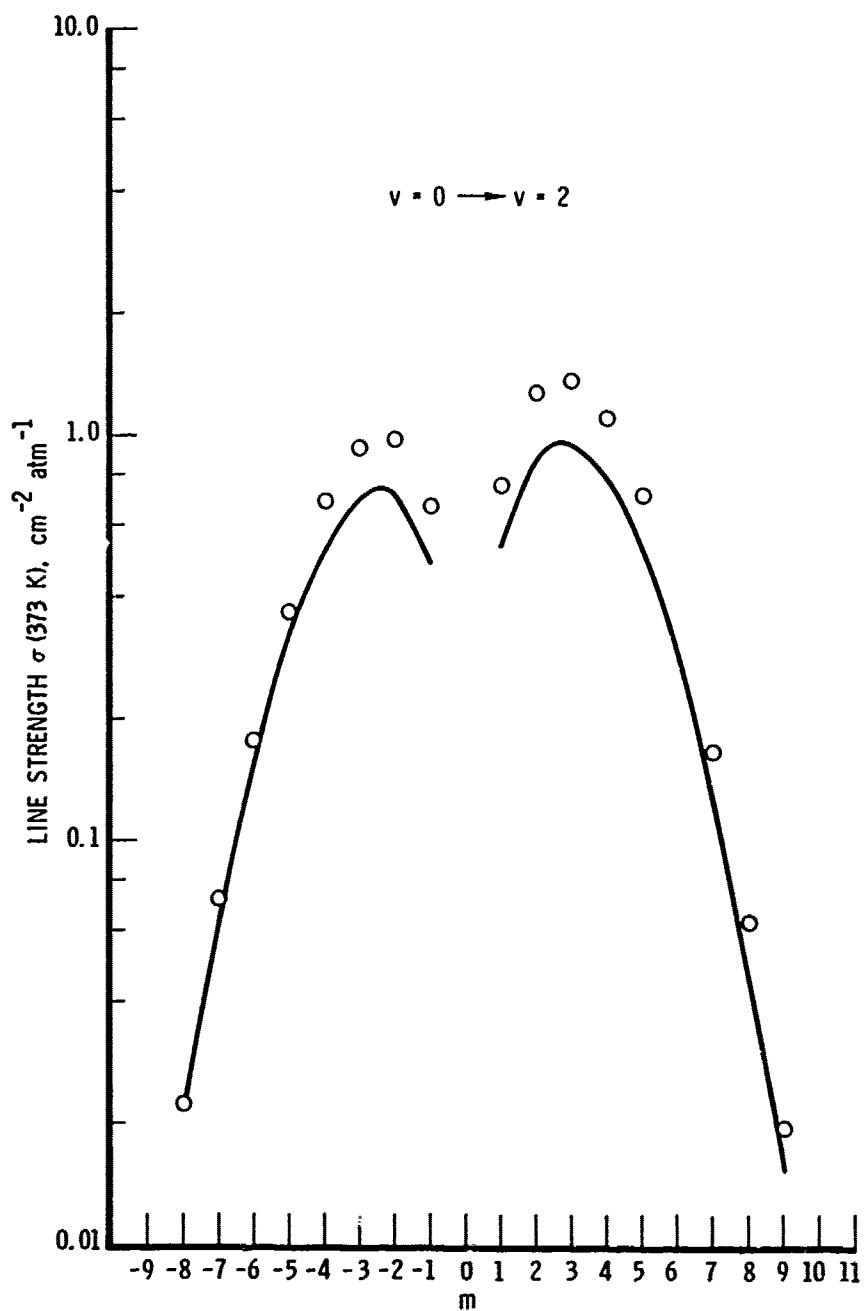


Figure 16. Comparison of Computed and Experimental HF Line Strengths for the 0-2 Band. The values obtained in the present study are connected by a solid curve. Experimental values from the work of Meredith²⁸ are shown (O).

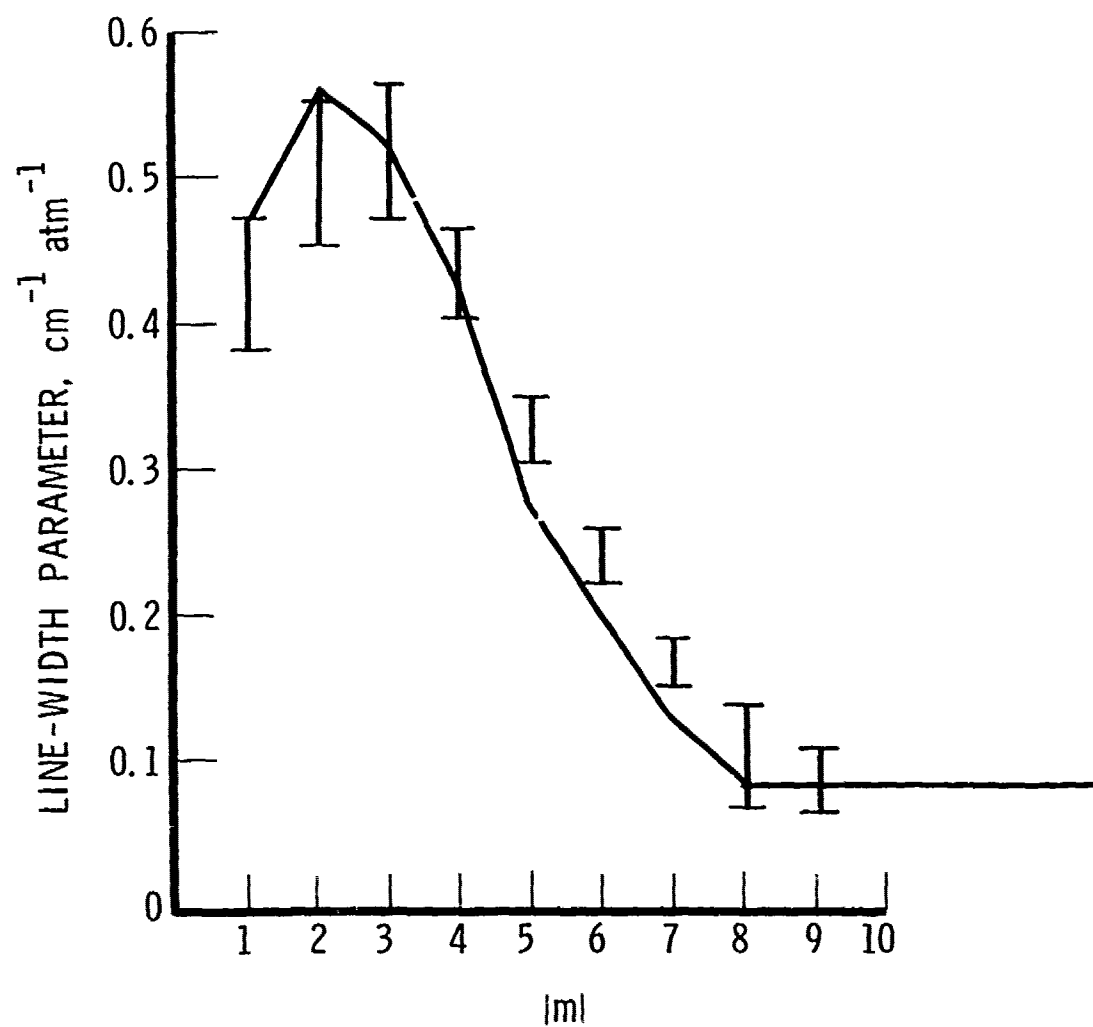


Figure 17. Summary of HF Experimental Line-Width Parameter Data. The vertical bars indicate the range of the values observed by various investigators and listed in Table 7. The values used in the present study are connected by straight line segments.

Table 7. HF Line-Width Parameter Data^a

m	R		P		R		P		R		P		Present Work
1	0.405		0.382	0.384	0.425	0.472	0.458	0.473	0.42				0.47
2	0.454		0.471	0.468	0.476	0.529	0.501	0.553	0.51				0.56
3	0.471		0.483	0.493	0.474	0.528	0.563	0.547	0.53				0.52
4	0.403	0.432	0.407	0.412	0.422	0.427	0.454	0.465	0.45				0.42
5	0.305	0.327	0.323	0.317	0.347	0.317	0.345	0.337	0.34				0.28
6	0.225	0.239	0.235	0.240		0.237	0.259	0.223	0.25				0.20
7	0.152	0.168	0.155	0.165	0.182	0.185	0.173		0.18				0.13
8	0.068		0.118	0.115	0.141	0.138							0.084
9	0.065				0.101	0.109							0.084
Temperature, K		390		390		373		373					390
Ref.		27		22		28		26					23

^a Values are in $\text{cm}^{-1} \text{atm}^{-1}$

to 390 K as in the program of Randall¹ and are shown connected by straight line segments. As with HCl, a 20-percent variation in experimental values is observed. The effect of the change with temperature of the $|m|$ dependence of the line-width parameter, which is not included in the present calculations, is also apparent.

Of the several parameters in the halide line-parameter compilations, the line width is the least accurate. Theoretical models of pressure broadening are available.²⁹ Although the results are not in complete agreement with measured values (Fig. 11), the application of a consistent theory for extrapolation, rather than the ad hoc procedures used here, is certainly preferable for improvement of the line width values. Simple methods for incorporating the variation in J dependence with temperature should also be incorporated in the spectral calculation programs.

The results of an independent study similar to the present one for the $\Delta v = 1$ bands of HF and DF were recently published by Goldman et al.³⁰ Their basic data sources were the same as those used here. Their line parameters were published as a table of line strengths (σ) at 1273 K. The line strengths for the 2-3 band of HF are compared in Fig. 18, where the solid curve represents the results of the present study, and the dashed curve represents those of Goldman. The P-branch results are indistinguishable on the scale of the figure. Goldman's R-branch results are a few percent lower than our results, but certainly agree to within the accuracy quoted for either set of results.

C. HF SPECTRAL COMPARISON

The final measure of the adequacy of a line-parameter compilation for spectral computation is the comparison of computed and experimental spectra. In Fig. 19 are shown the spectra computed for a 60-cm sample of HF at 1 atm and with the inhomogeneous temperature distribution shown in Fig. 20. The spectra presented are the result of convolving a 4.5-cm^{-1} wide FWHM triangular instrument function with the computed high-resolution

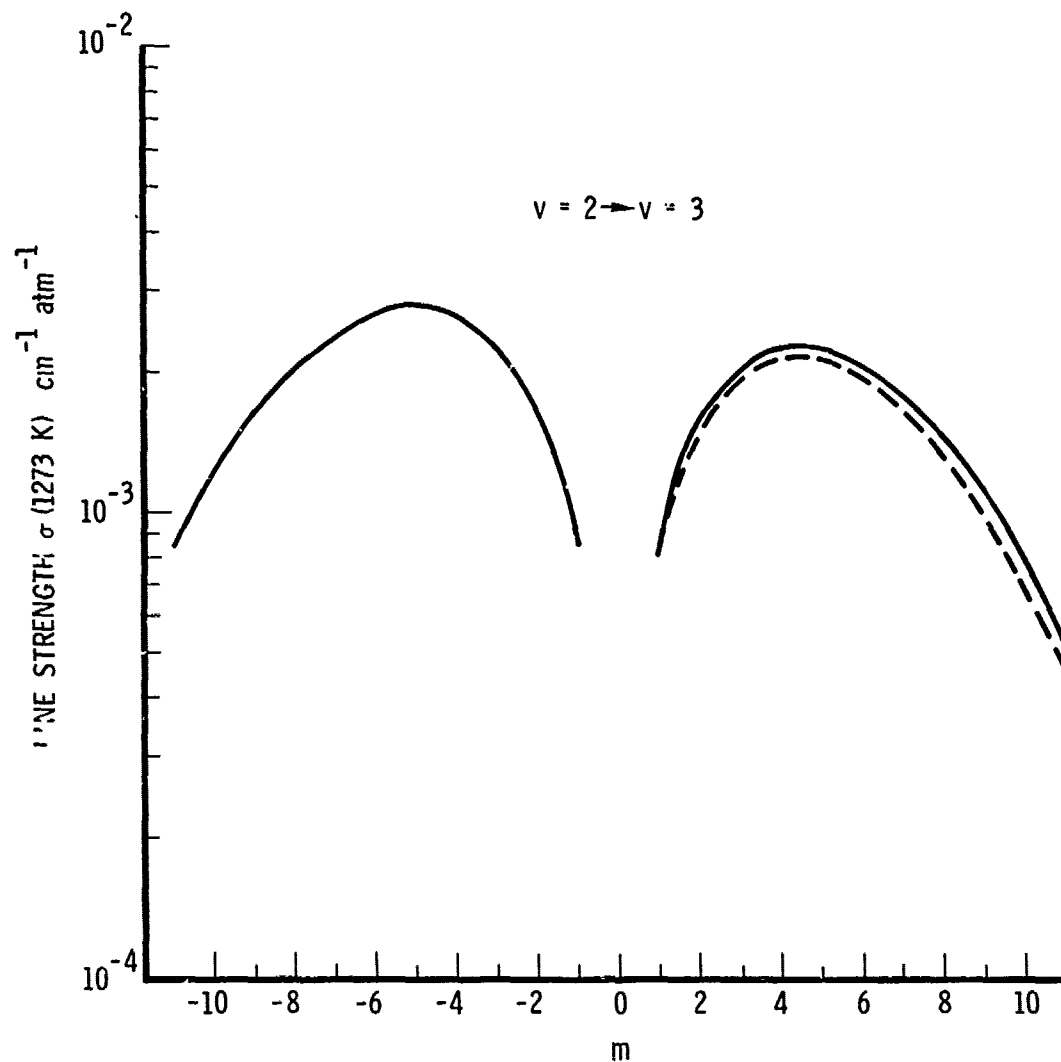


Figure 18. Comparison of the Computed HF Line Strengths of Goldman, et al. at 1273 K with Values from the Present Study in the 2-3 Band. The solid curve represents results of the present study. Goldman's results are denoted by a broken curve, which is indistinguishable from the solid curve in the P branch.

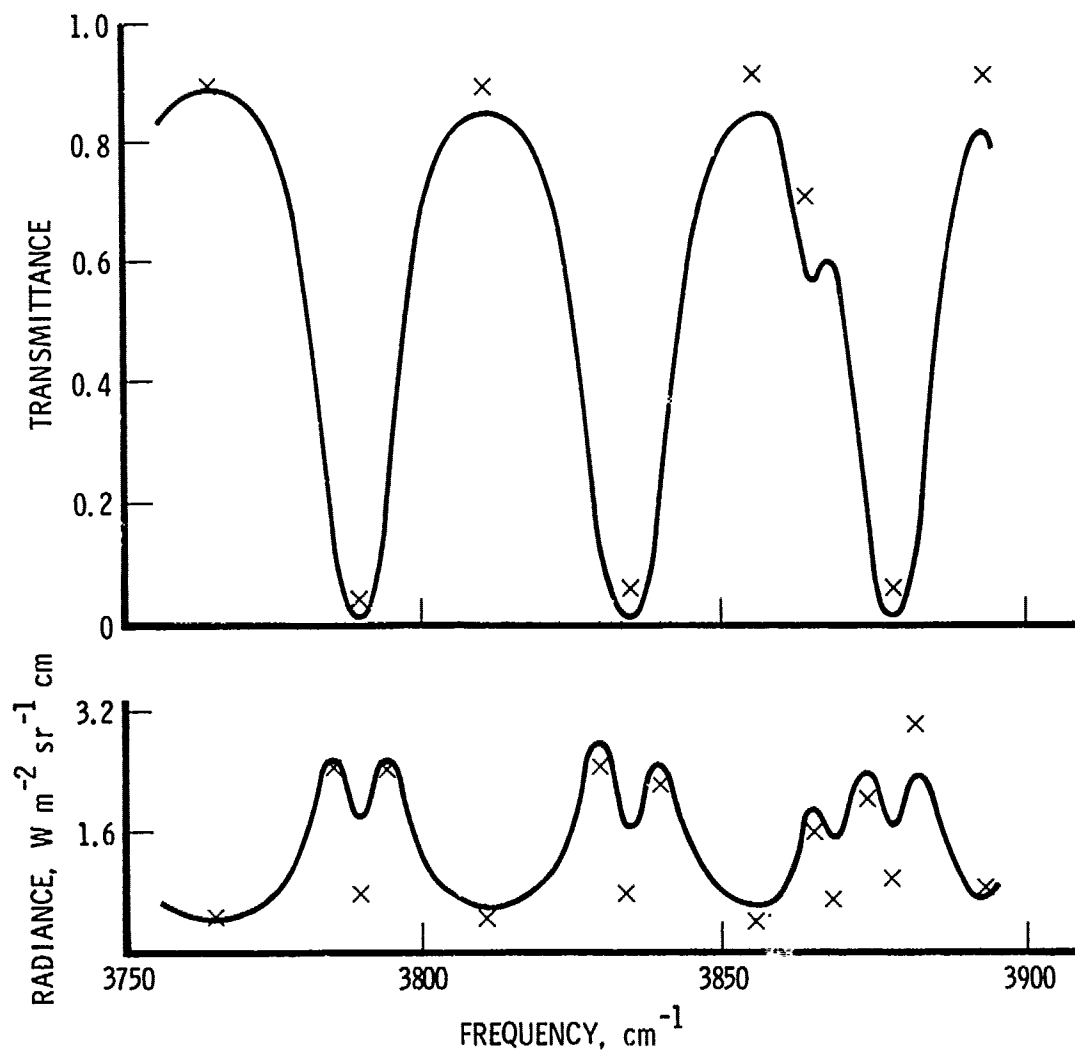


Figure 19. Comparison of Experimental and Computed Characteristics of a Nonisothermal HF Sample. The solid curve is the computed transmittance and radiance for a path with the temperature profile as shown in Fig. 20. Comparable experimental values from the work of Simmons⁵ are shown (X).

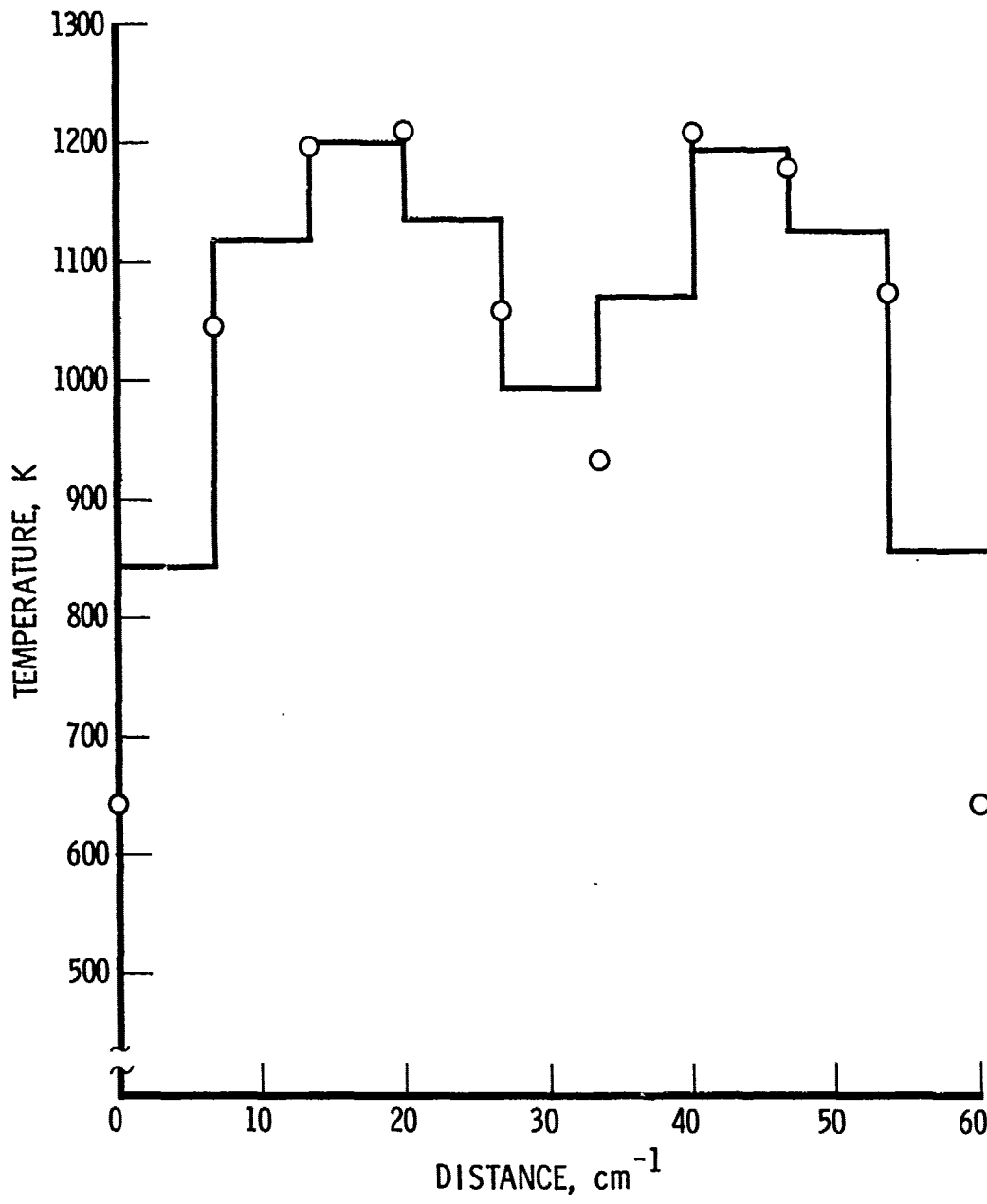


Figure 20. Temperature Profile for Nonisothermal HF Computation. The measured temperatures along the sample cell used to obtain the experimental points in Fig. 19 are shown (O). The horizontal line segments denote the temperature profile used to simulate the sample for computation.

spectrum. These conditions agree with experimental spectra obtained by Simmons, Yamada, and Arnold.⁵ Because the experimental spectra do not lend themselves to reproduction, we have extracted the extreme values from the experimental spectra and plotted them in Fig. 19. The agreement is quite satisfactory.

IV. HOT-GAS SPECTRA

In this section, the spectral line parameters for HCl and HF discussed in Section III are combined with the AFCRL line parameter collection evaluated in Section II and used with the program described in Ref. 1 to compute the radiance from a path through two samples of hot gases characteristic of possible plume conditions. The radiance at the plume boundary is evaluated, and the radiance available after passing through an absorbing atmospheric path is computed. The ratio of spectrally degraded apparent radiance to plume radiance demonstrates the importance of including the effects of the source spectrum when considering the propagation of radiation through the atmosphere.

The conditions for the two gas samples, designated here as plumes A and B, are summarized graphically in Figs. 21 and 22. The conditions represented by the solid curves were supplied by R. H. Lee* and are based on complicated plume flow field modeling studies. These curves describe the radial profile of temperature and species concentration of an assumed cylindrically symmetric gas sample at an axial location in the sample near the position of peak infrared emission. The samples differ mainly in composition. The radiating species in plume A are CO, CO₂, and H₂O, whereas those in plume B are HCl and HF. Both plumes are assumed to be at a constant pressure of 55.3 mb.

The computation of radiance for inhomogeneous samples such as those discussed here is approximated by a sequence of homogeneous segments. The values selected for this simulation are shown in Figs. 21 and 22 by the horizontal lines. The segments are not the same geometric length, but, rather, the total number of molecules in each segment is approximately the

*R. H. Lee, private communication (1975).

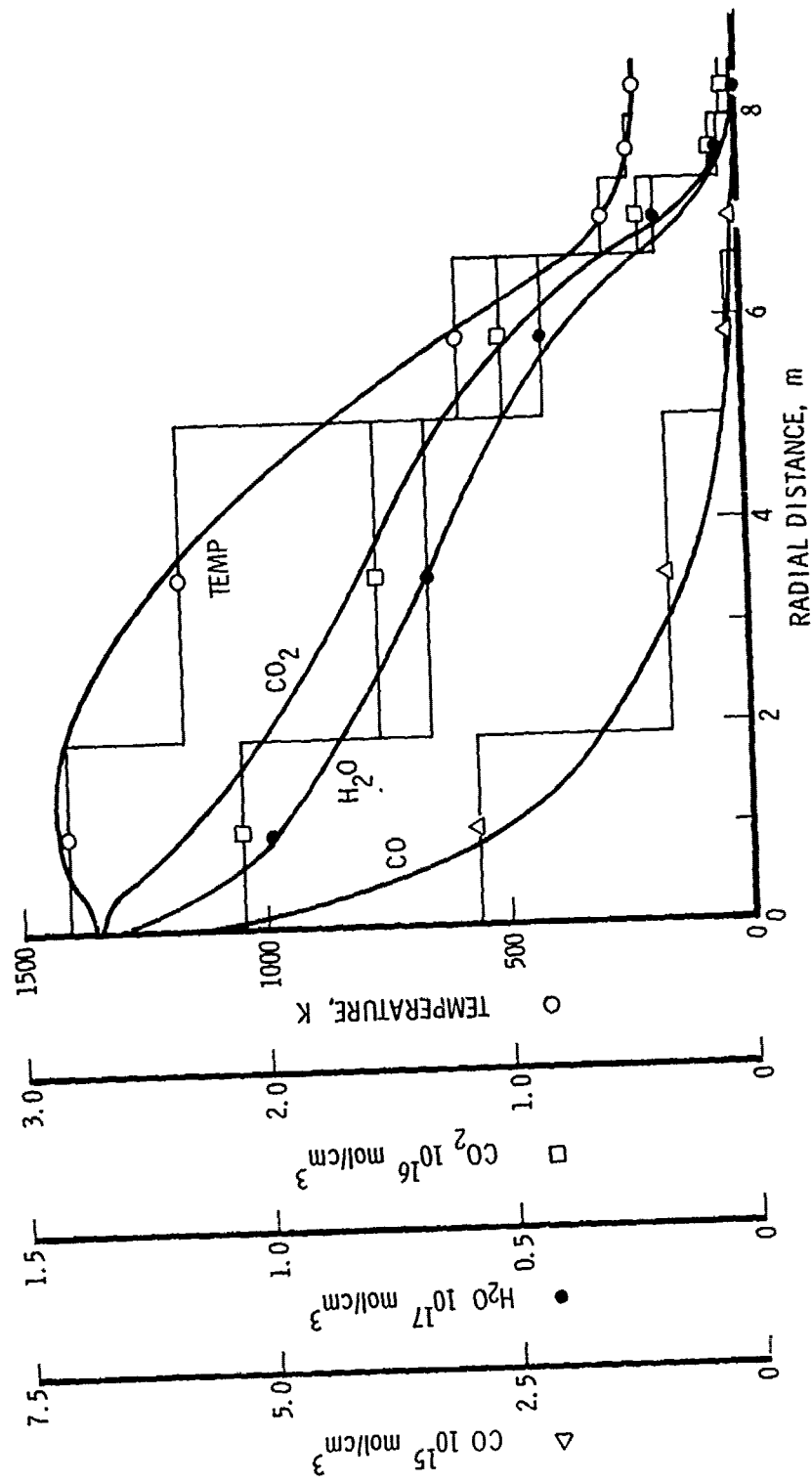


Figure 21. Temperature and Species Concentrations for Plume A. The solid curves denote radial profiles of the concentrations of H₂O, CO₂, CO, and the temperature. The horizontal line segments indicate the homogeneous values of these parameters used to simulate the radial profiles. Note that each of the four parameters has a different ordinate scale.

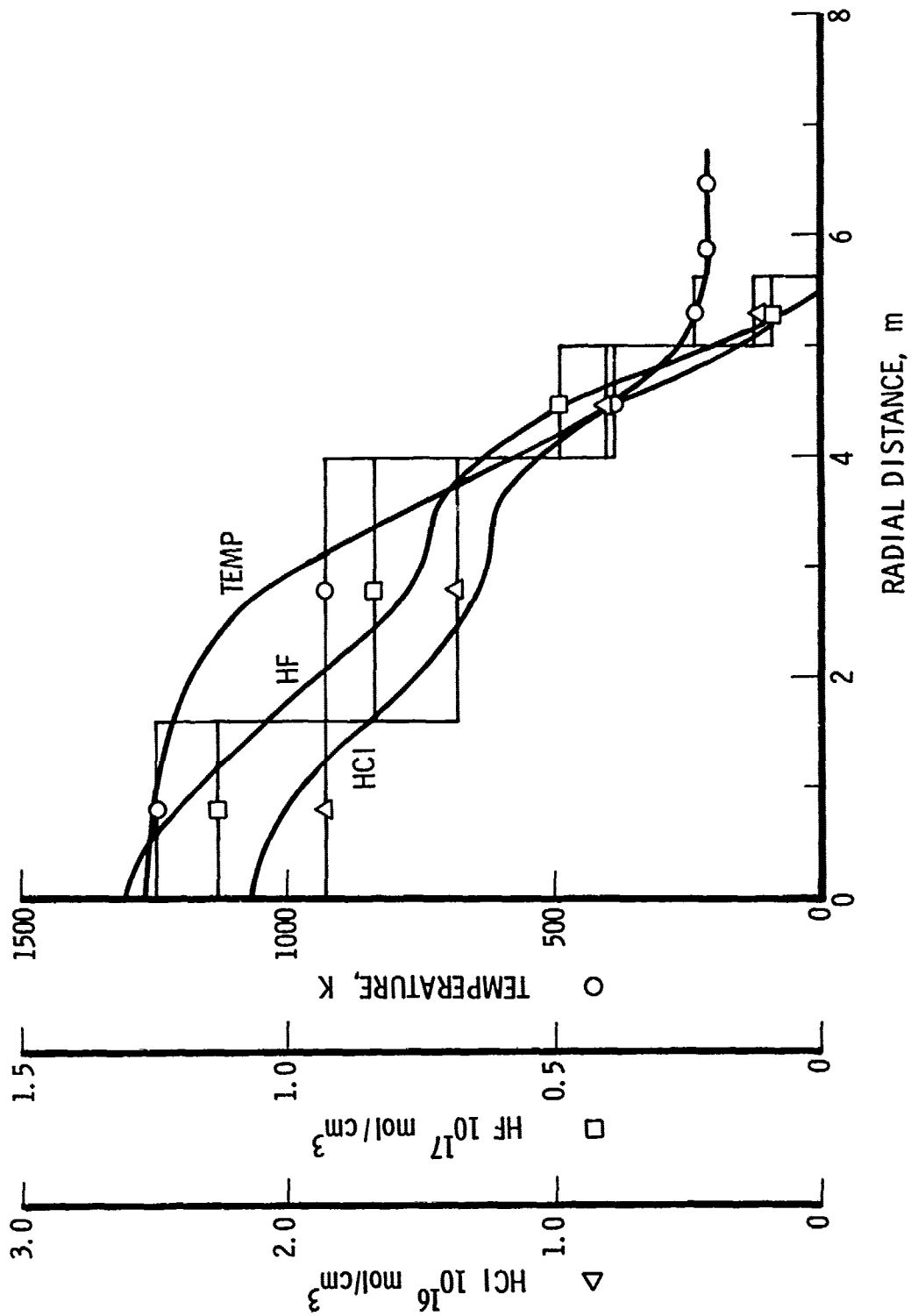


Figure 22. Temperature and Species Concentrations for Plume B. The solid curves denote the radial profiles of the concentrations of HF, HCl, and temperature. The horizontal line segments indicate the homogeneous values of these parameters used to simulate the radial profiles. Note that each of the three parameters has a different ordinate scale.

same. Earlier studies have indicated that this provides a better simulation than equal geometric length segments. The numerical values used in the computations are given in Tables 8 and 9 for half of the assumed symmetric plume.

The atmospheric model used to attenuate the radiances consists of a path from 20 km to space at a 60-deg zenith angle through a mid-latitude summer model atmosphere.³¹ Continuum absorption in the atmosphere was ignored.

All computations of spectra were carried out with the INHOM program¹ at a resolution of 0.01 cm^{-1} for the entire spectral region from 2 to $5 \mu\text{m}$ ($2000\text{-}5000 \text{ cm}^{-1}$). Samples of the plume radiance for plumes A and B are shown in Figs. 23 and 24. Apparent radiance spectra were obtained by multiplying the high-resolution plume radiance spectrum by the high-resolution atmospheric transmittance spectrum. The result was a spectrum of the plume radiance that reached the top of the atmosphere. The atmospheric radiance was not added. The resulting high-resolution radiance spectra

Table 8. Plume A Simulation Conditions

Radial Limits, m	Temperature, K	Column Densities, 10^{17} mol/cm^2		
		H ₂ O	CO ₂	CO
-1.89 to +1.89	1403.45	371.531	78.866	10.587
1.89 to 5.023	1165.40	205.423	47.677	2.546
5.023 to 6.601	586.48	64.962	15.553	0.263
6.601 to 7.352	279.38	12.827	3.074	0.063
7.352 to 7.966	227.82	2.771	0.627	0
7.966 to 8.534	211.37	0.341	0.324	0

Table 9. Plume B Simulation Conditions

Radial Limits, m	Temperature, K	Column Densities, 10^{16} mol/cm ²	
		HCl	HF
-1.614 to +1.614	1245.01	598.402	3642.22
1.614 to 4.007	923.31	324.999	1994.34
4.007 to 5.017	389.54	80.383	494.963
5.017 to 5.627	235.37	9.170	56.405
5.627 to 6.188	216.70	0.230	1.409
6.188 to 6.75	216.70	0	0.001

were convolved with triangular instrument functions of two different widths, 2 and 20 cm⁻¹ FWHM, and are shown in Figs. 25 through 34. The low-resolution atmospheric transmittance spectra are shown in Figs. 25 and 26; the low-resolution plume A radiance spectra are shown in Figs. 27 and 28; the low-resolution apparent plume A radiance spectra are shown in Figs. 29 and 30; the low-resolution plume B radiance spectra are shown in Figs. 31 and 32; the low-resolution apparent plume B radiance spectra are shown in Figs. 33 and 34. Figures 31 through 34 have the same vertical scale in order to emphasize the reduction in average radiance of plume B compared with that of plume A because of the lower density of lines. Thirty-two times the values of the 20-cm⁻¹ resolution radiance is also plotted for assistance in determining quantitative values if desired.

The dependence of the effective atmospheric transmittance spectrum on the source spectrum is emphasized in Figs. 35 and 36. The solid curve represents the 20-cm⁻¹ resolution average transmittance identical to the curves in Figs. 25 and 26. The dashed and broken curves were obtained by calculating the effective average transmittance

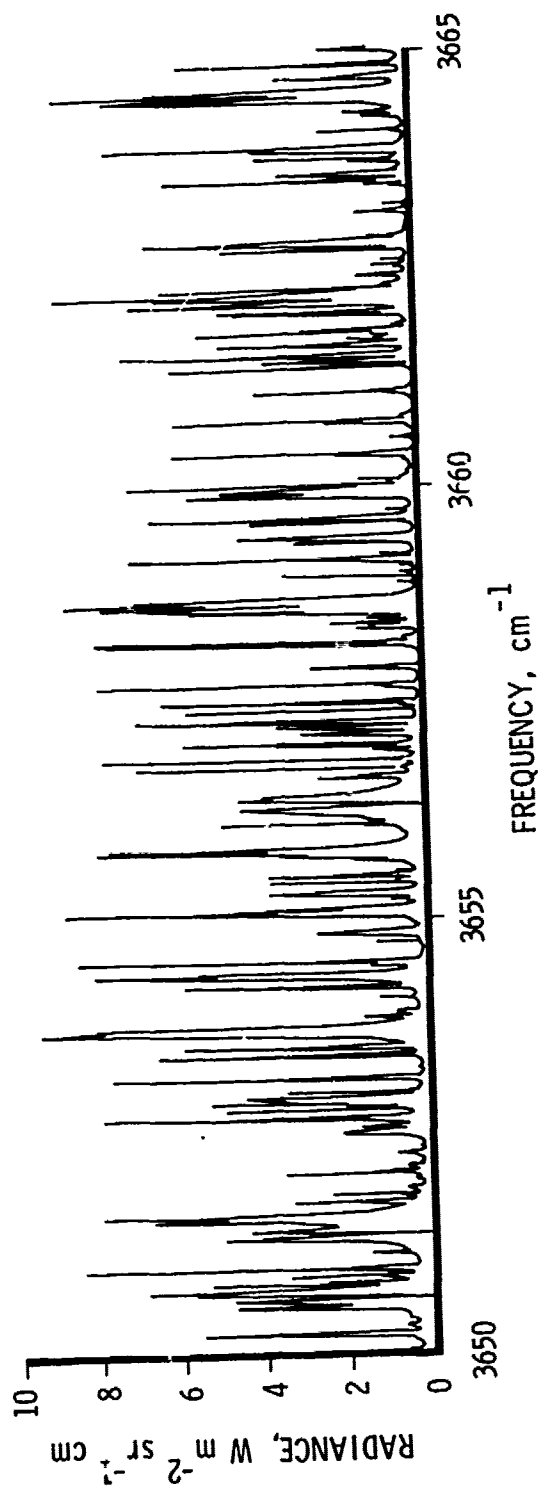


Figure 23. Segment of the High-Resolution Plume A Radiance Spectrum

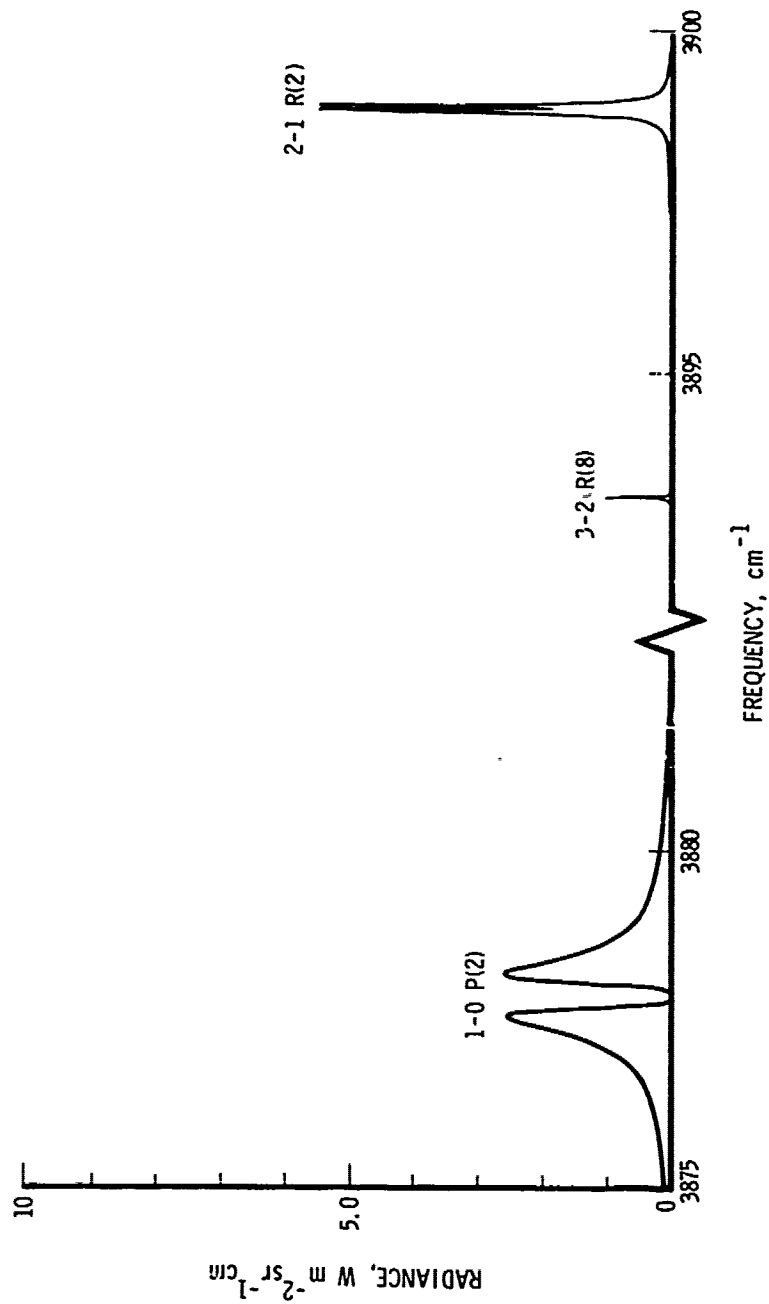


Figure 24. Segment of the High-Resolution Plume B Radiance Spectrum in the HF Emission Region

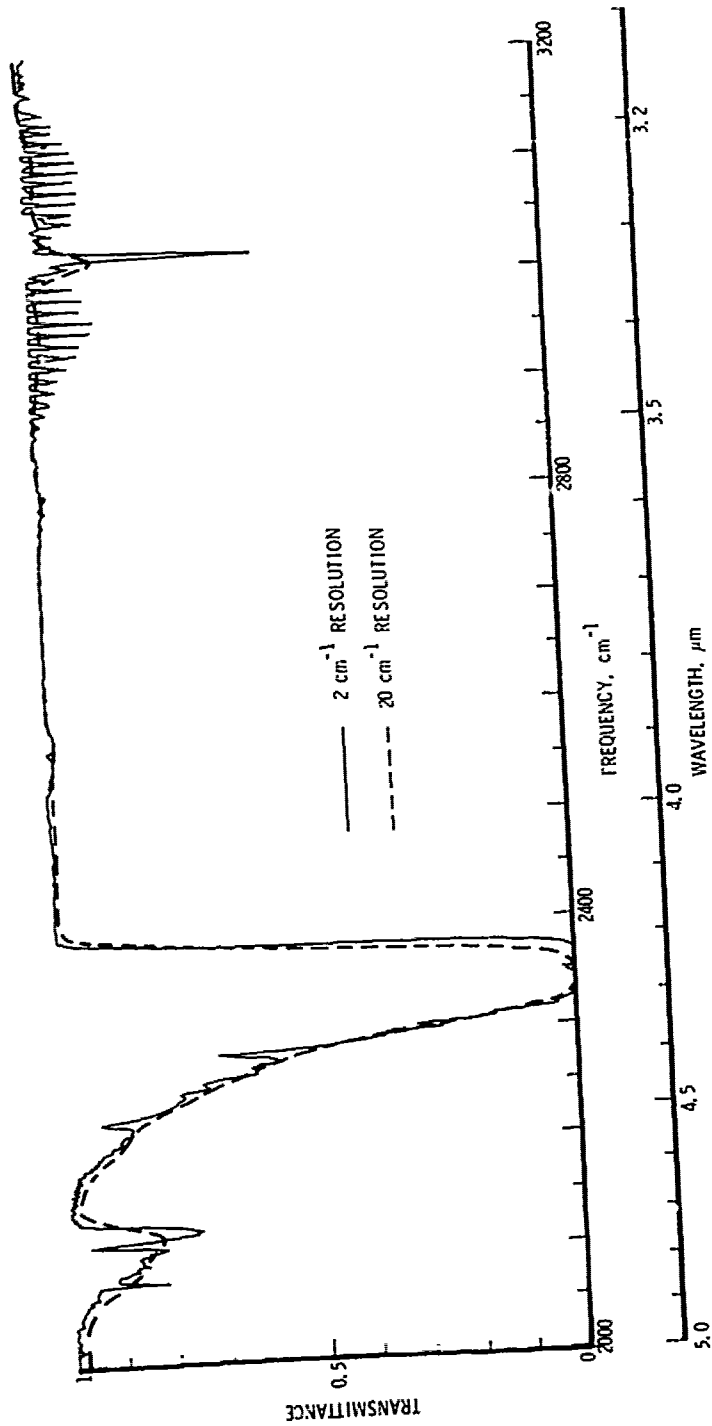


Figure 25. Computed Atmospheric Transmittance Between 2000 and 3200 cm^{-1} . The high-resolution transmittance spectrum for a path from 20 km to space at a 60 deg zenith angle through a mid-latitude summer model atmosphere has been convolved with two different triangular instrument functions.

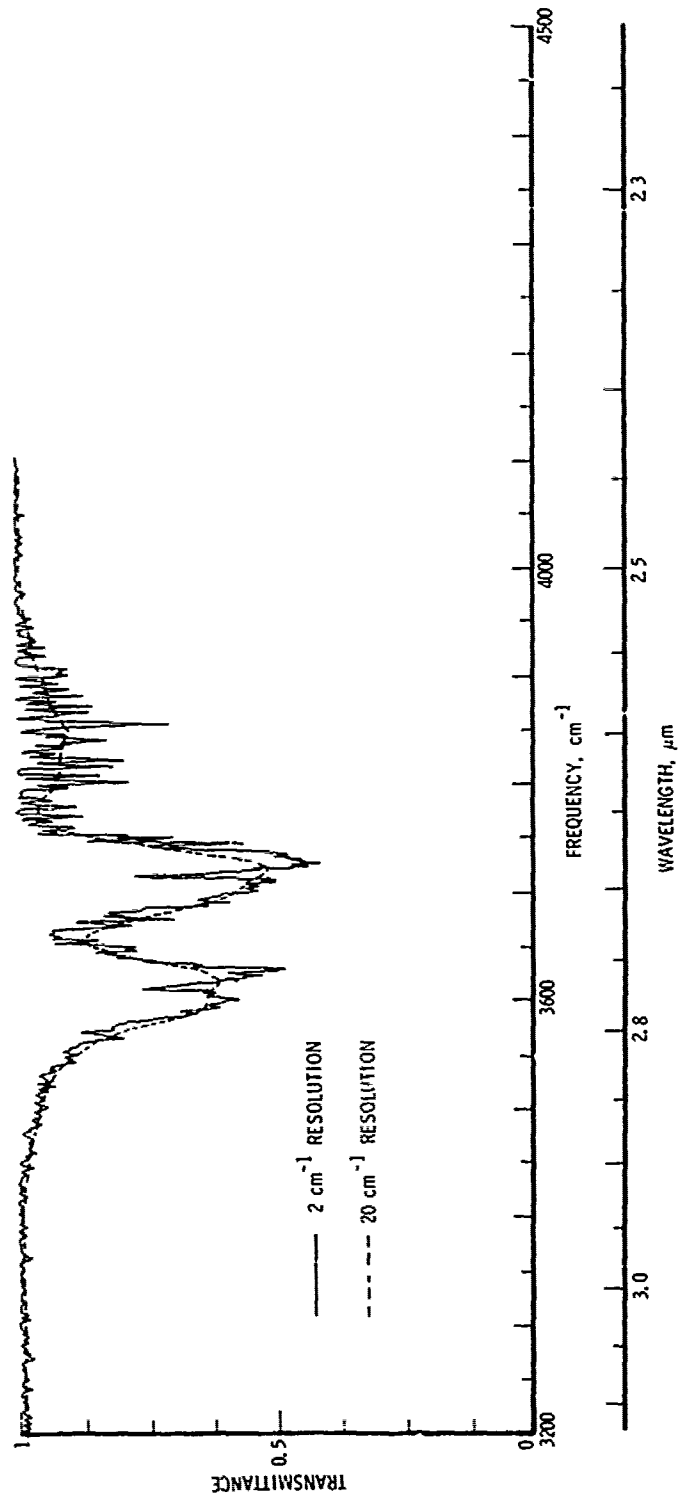


Figure 26. Computed Atmospheric Transmittance Between 3200 and 4100 cm^{-1} . The conditions are the same as for Fig. 25.

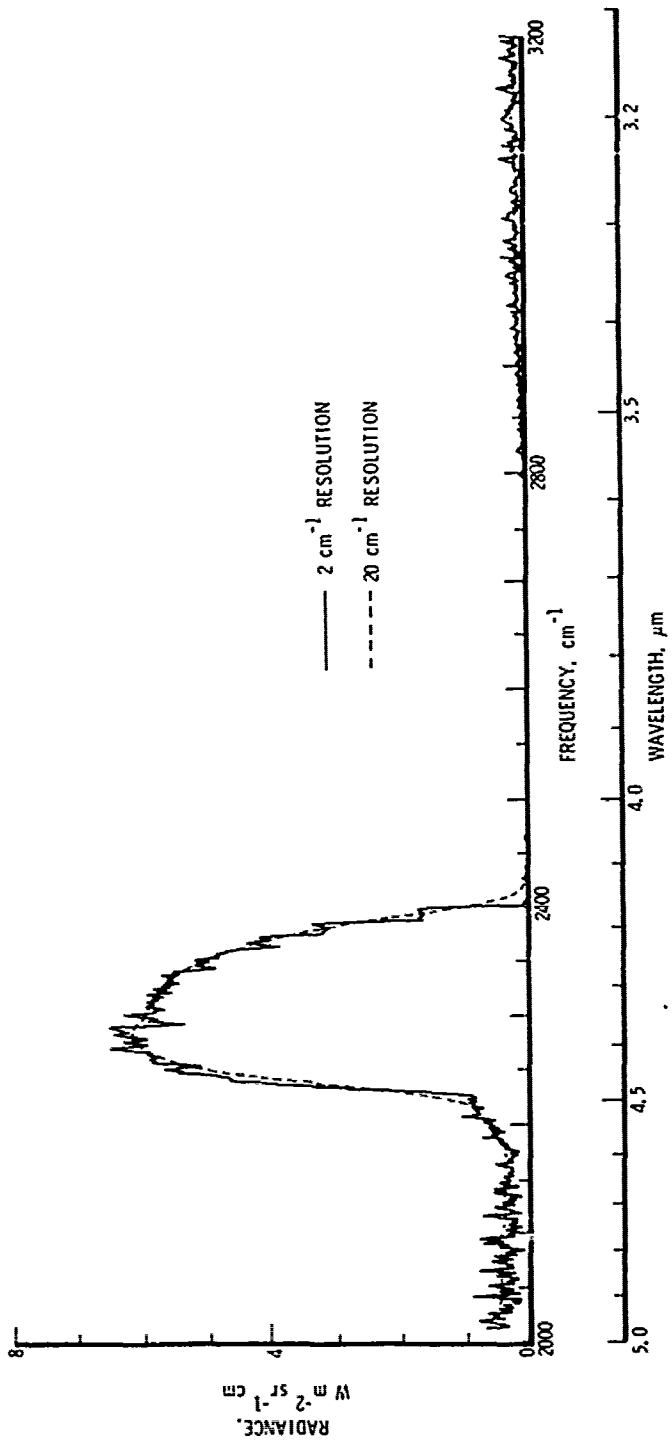


Figure 27. Computed Plume A Radiance Between 2000 and 3200 cm^{-1} . The high-resolution radiance spectrum for Plume A has been convolved with two different triangular instrument functions.

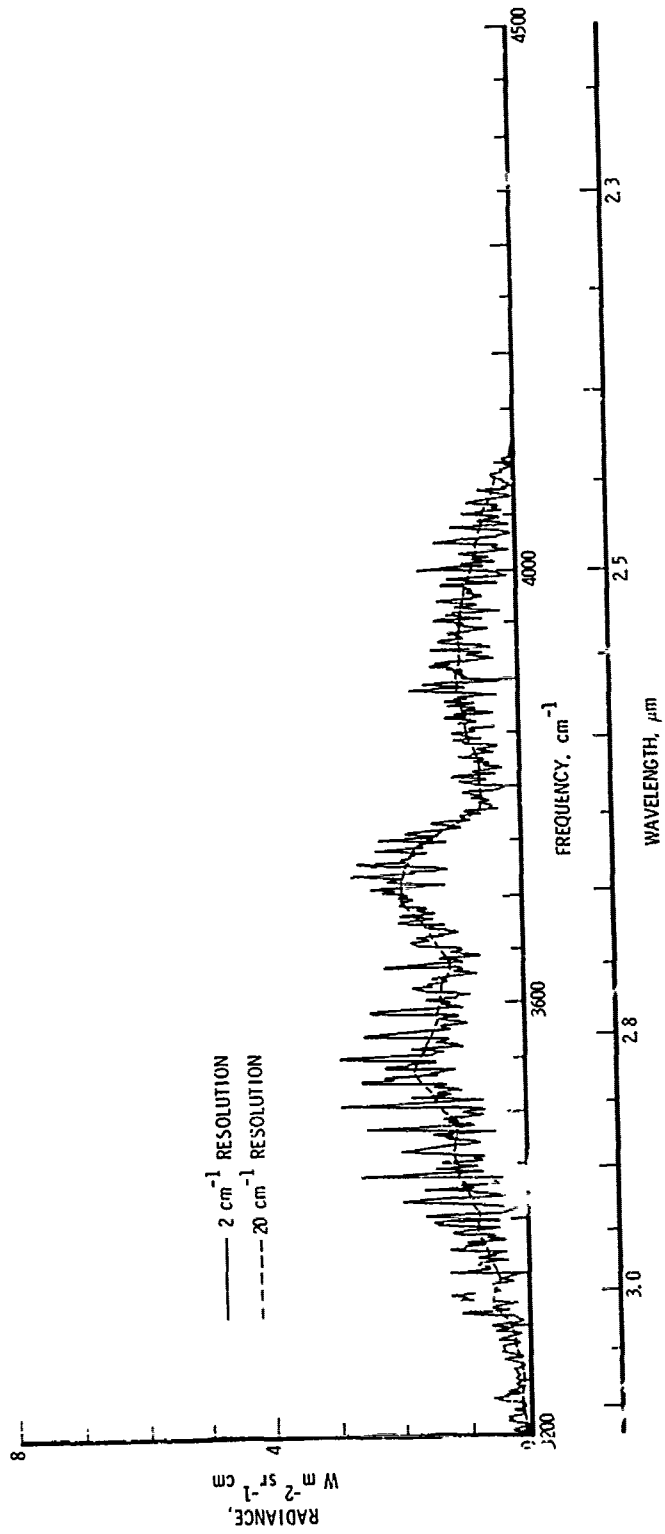


Figure 28. Computed Plume A Radiance Between 3200 and 4100 cm^{-1} . The conditions are the same as for Fig. 27.

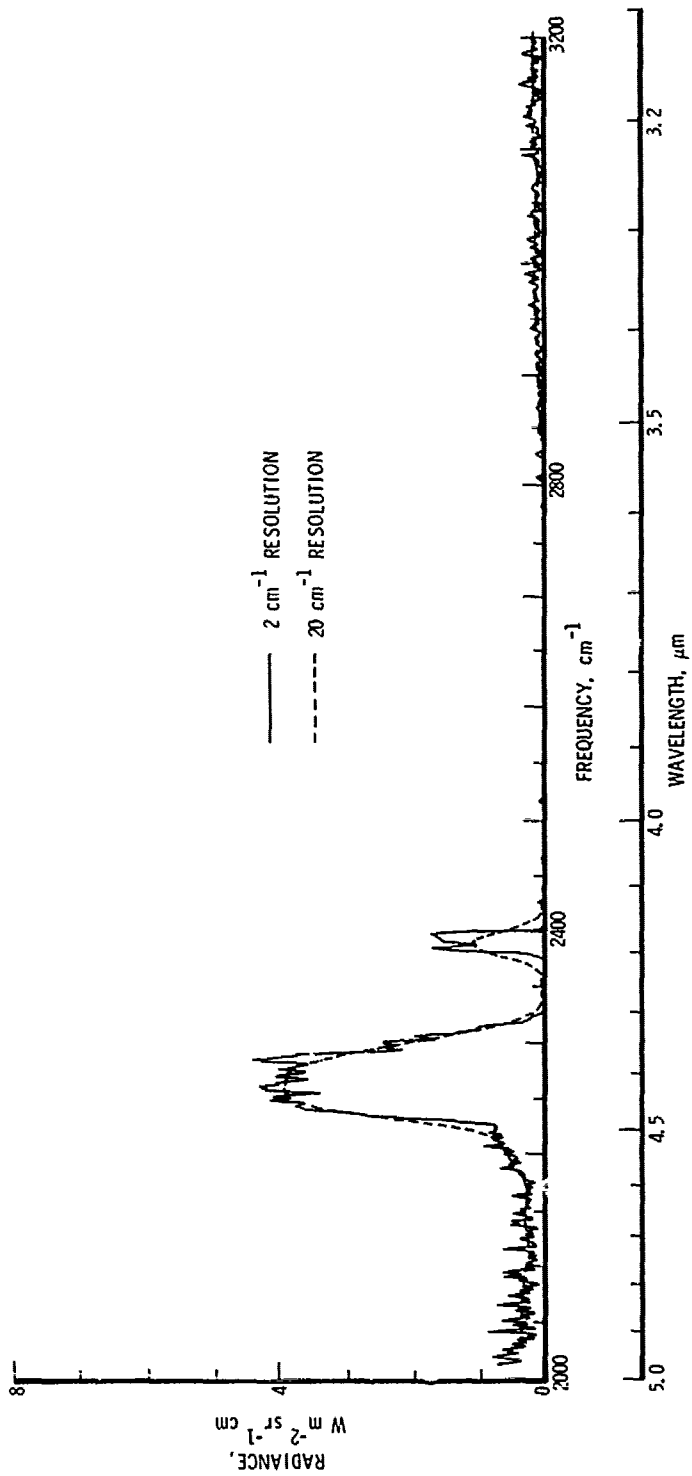


Figure 29. Apparent Plume A Radiance Between 2000 and 3200 cm^{-1} . The high-resolution Plume A spectrum has been multiplied by the high-resolution atmospheric transmittance spectrum on a point-by-point basis. The resulting spectrum, which describes the radiation from Plume A reaching the top of the atmosphere, has been convolved with two triangular instrument functions.

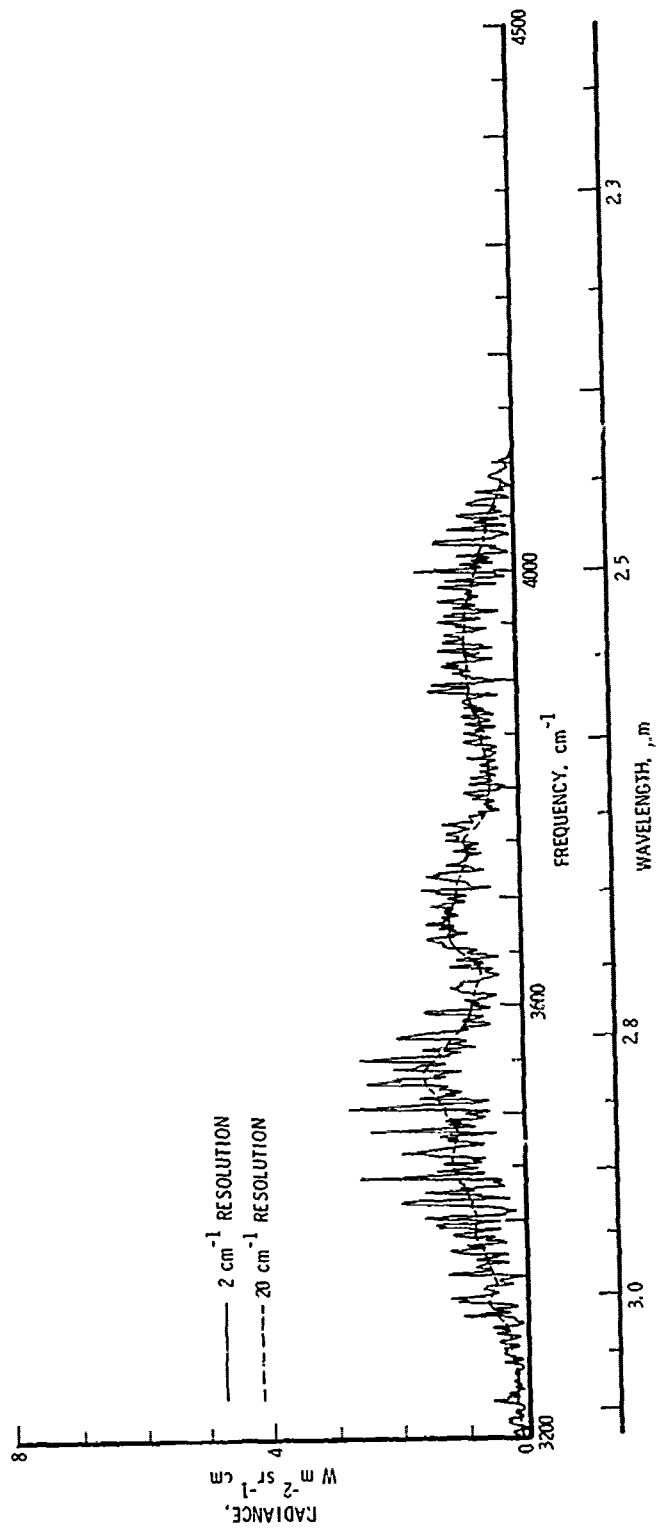


Figure 30. Apparent Plume A Radiance Between 3200 and 4100 cm^{-1} . The conditions are the same as for Fig. 29.

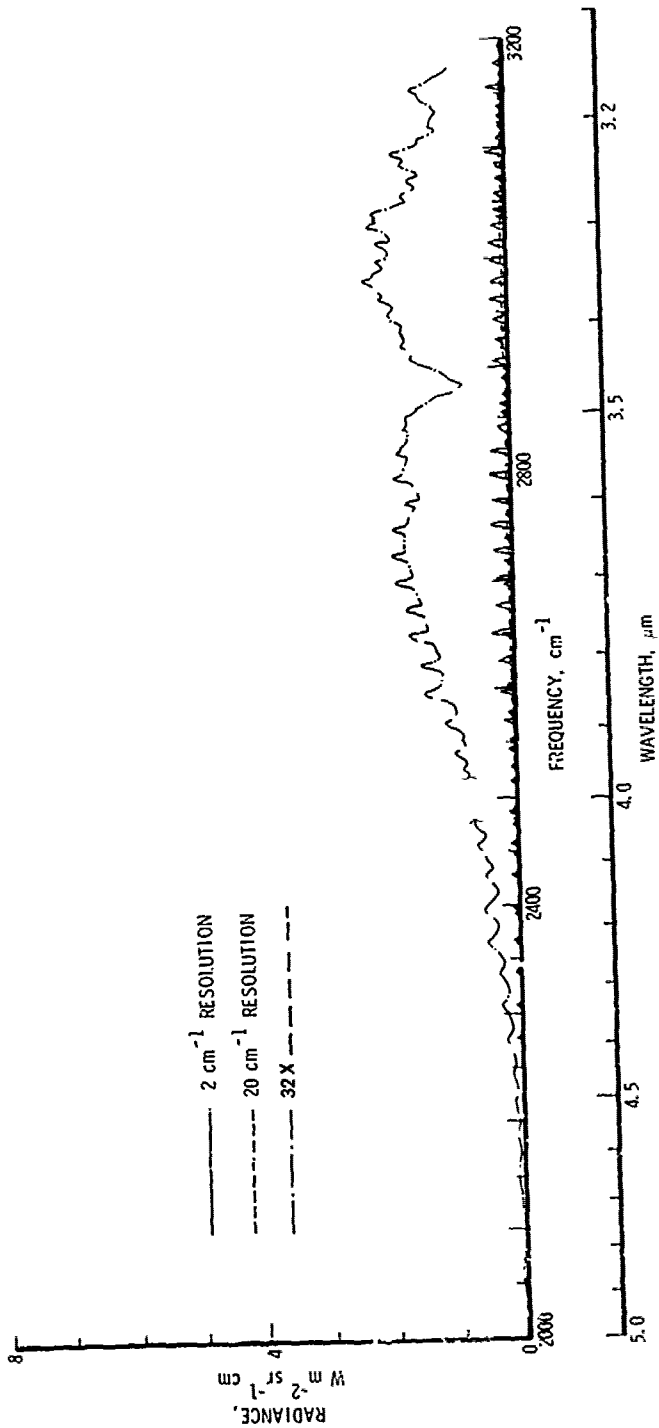


Figure 31. Computed Plume B Radiance Between 2000 and 3200 cm^{-1} . The high-resolution radiance spectrum from Plume B has been convolved with two different triangular instrument functions. The resulting spectra have been plotted with the same ordinate scale as Figs. 27 through 30 for easier comparison. The 20 cm^{-1} resolution spectrum is also plotted at 32 times magnification in order to facilitate the determination of quantitative values.

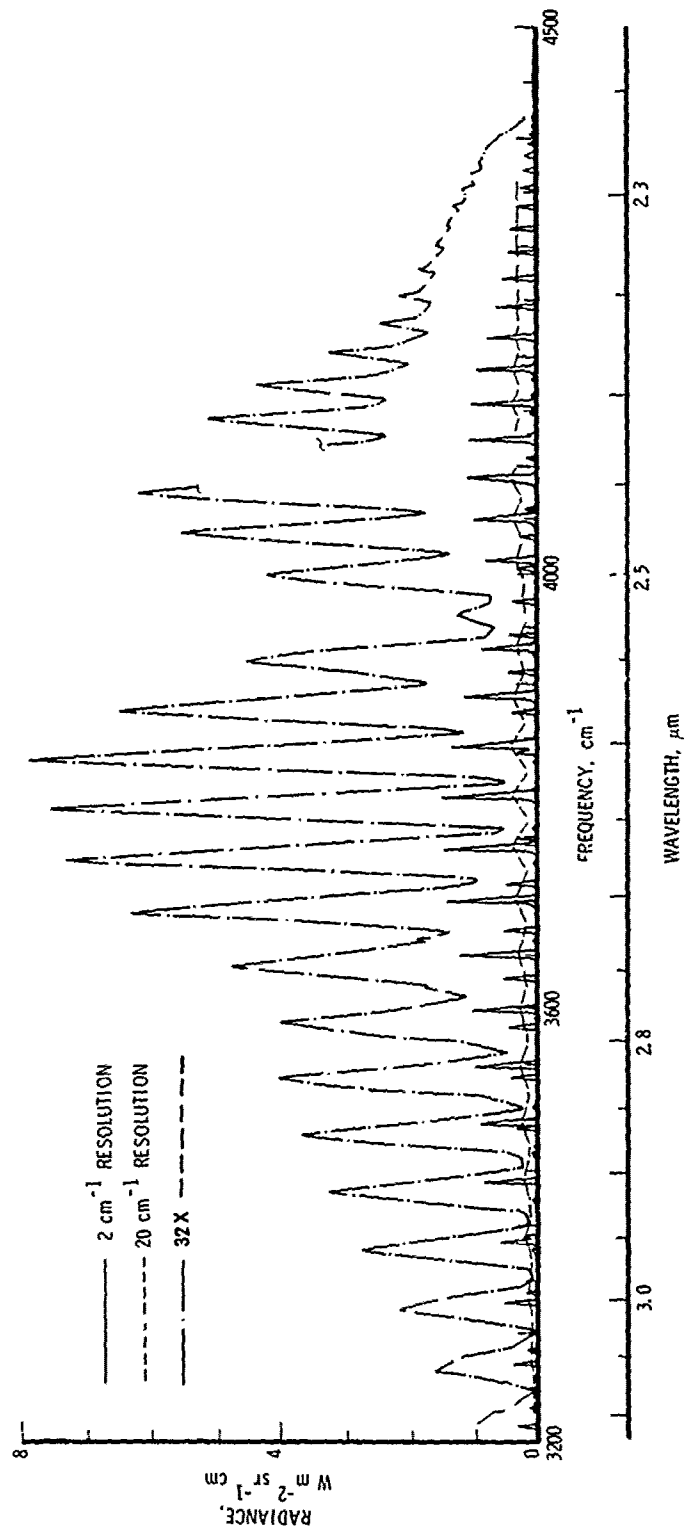


Figure 32. Computed Plume B Radiance Between 3200 and 4600 cm^{-1} . The conditions are the same as for Fig. 31.

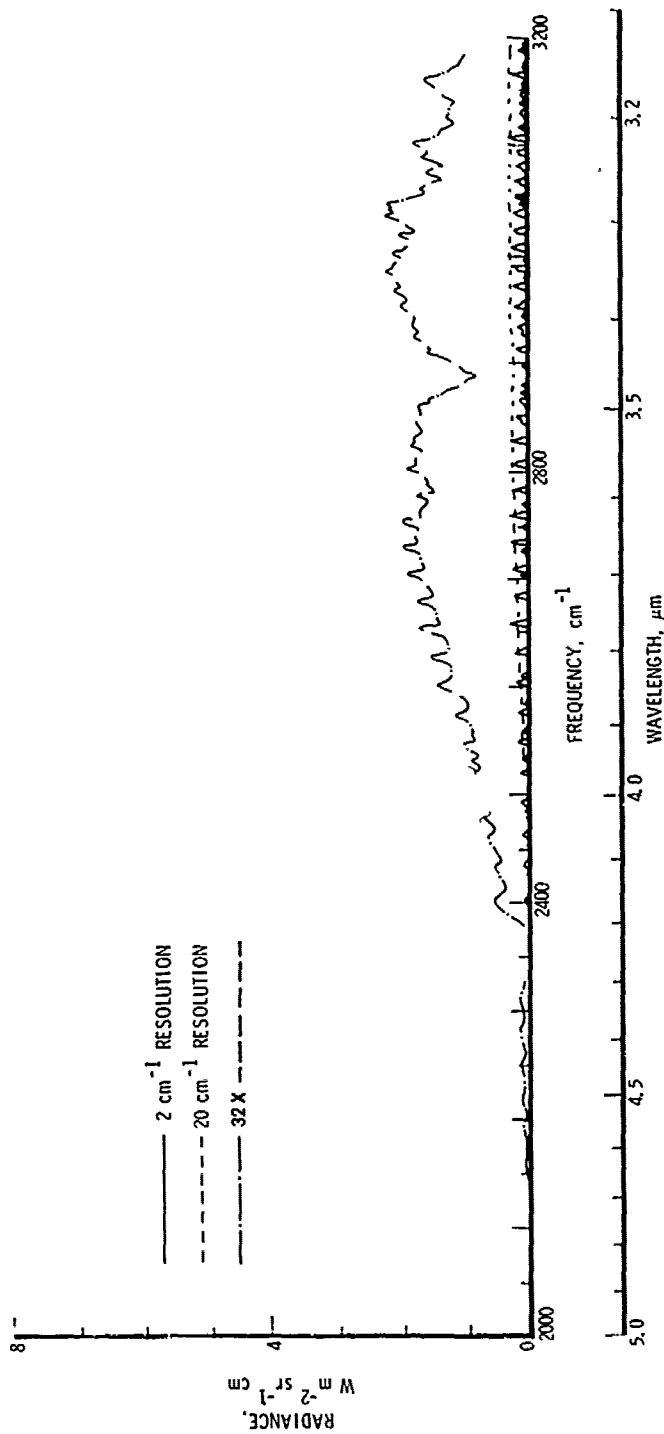


Figure 33. Apparent Plume B Radiance Between 2000 and 3200 cm^{-1} . The high-resolution Plume B spectrum has been multiplied by the high-resolution atmospheric transmittance on a point-by-point basis. The resulting spectrum, which describes the radiation from Plume B reaching the top of the atmosphere, has been convolved with two triangular instrument functions. The resulting spectra have been plotted with the same ordinate scale as Figs. 27 through 30 for easier comparison. The 20 cm^{-1} resolution spectrum is also plotted at 32 times magnification in order to facilitate the determination of quantitative values.

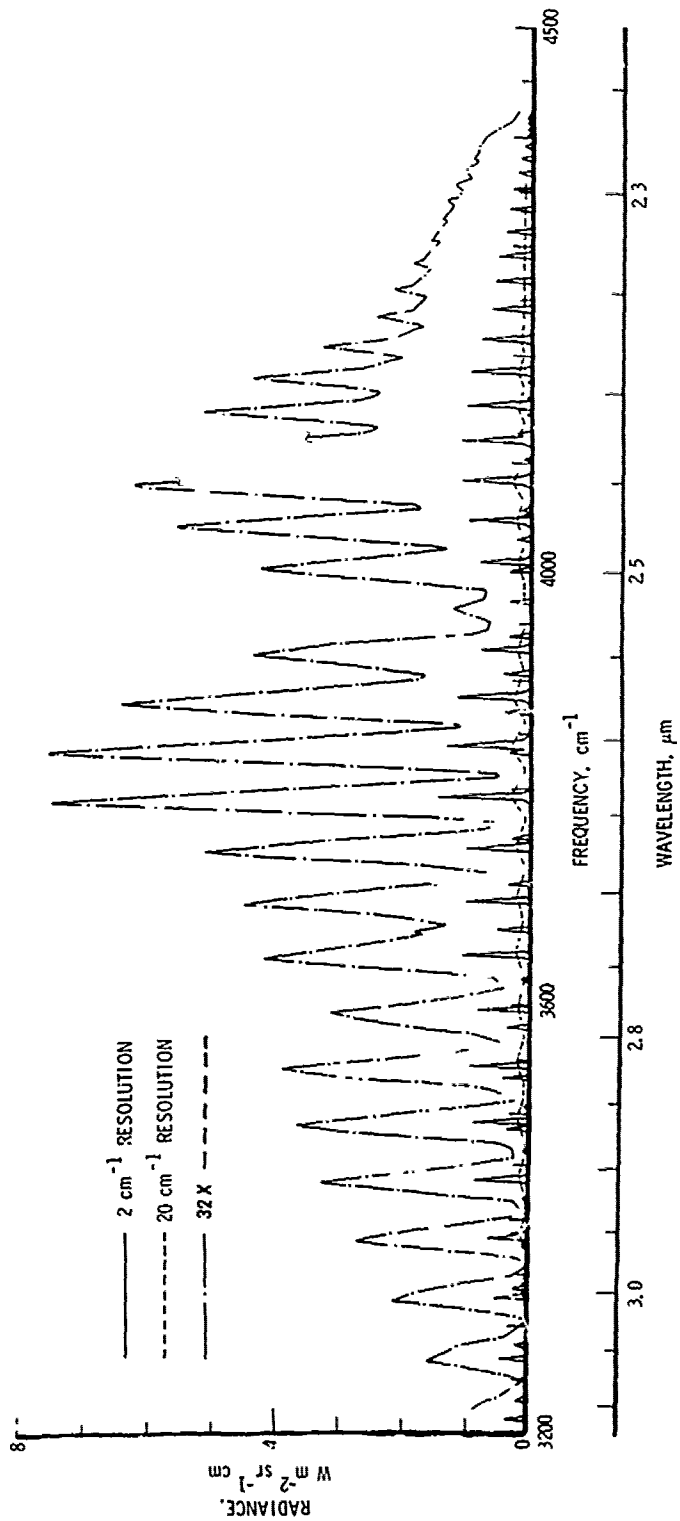


Figure 34. Apparent Plume B Radiance Between 3200 and 4400 cm^{-1} . The conditions are the same as for Fig. 33.

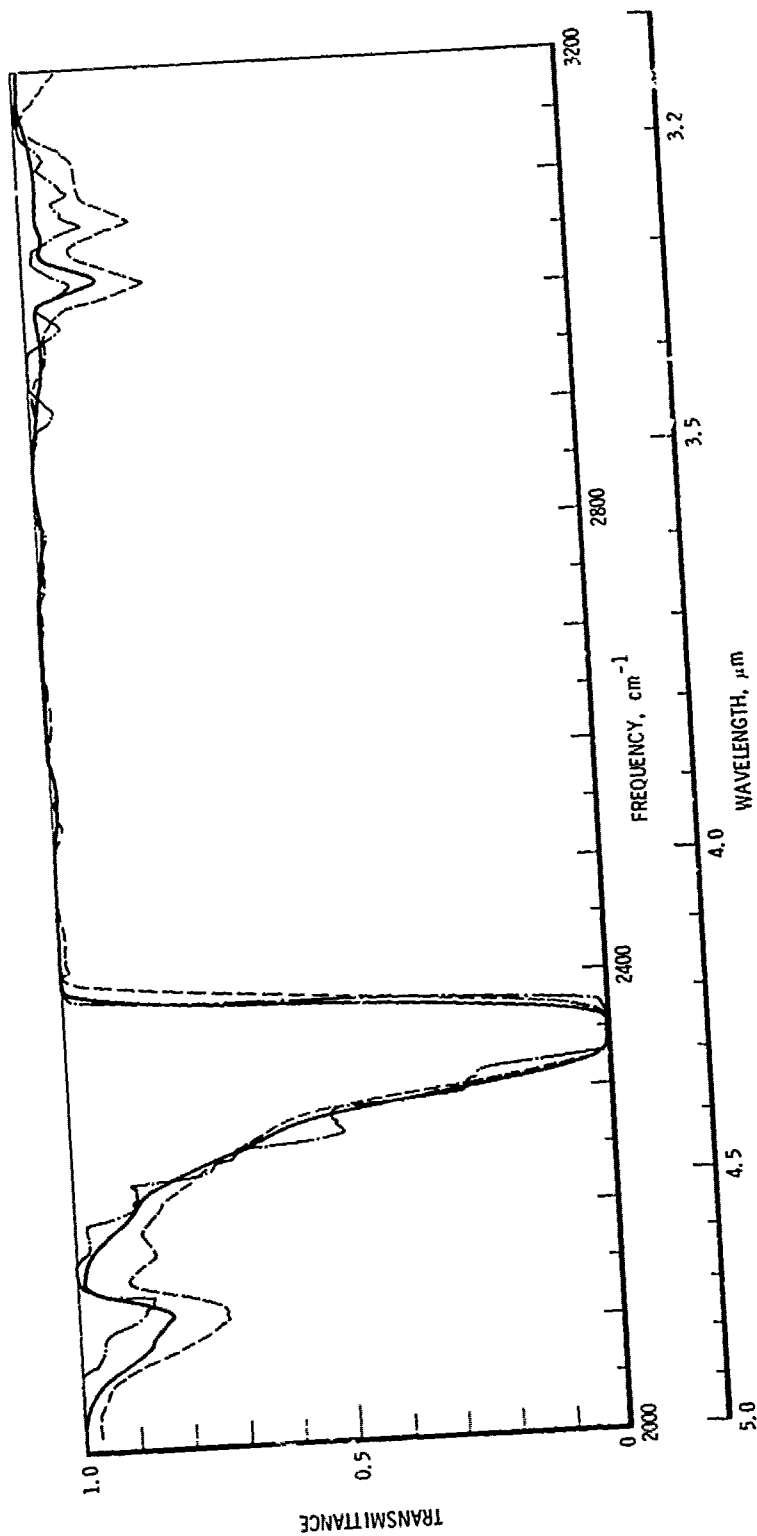


Figure 35. Dependence of Apparent Transmittance on Source Spectrum Between 2000 and 3200 cm^{-1} . The solid curve denotes the average atmospheric transmittance at 20 cm^{-1} resolution from Fig. 25. The dashed curve denotes the effective average transmittance for Plume A, which is the ratio of the 20 cm^{-1} resolution curve of Fig. 29 to that of Fig. 27. The broken curve denotes the effective average transmittance for Plume B, which is the ratio of the 20 cm^{-1} resolution curve of Fig. 33 to that of Fig. 31.

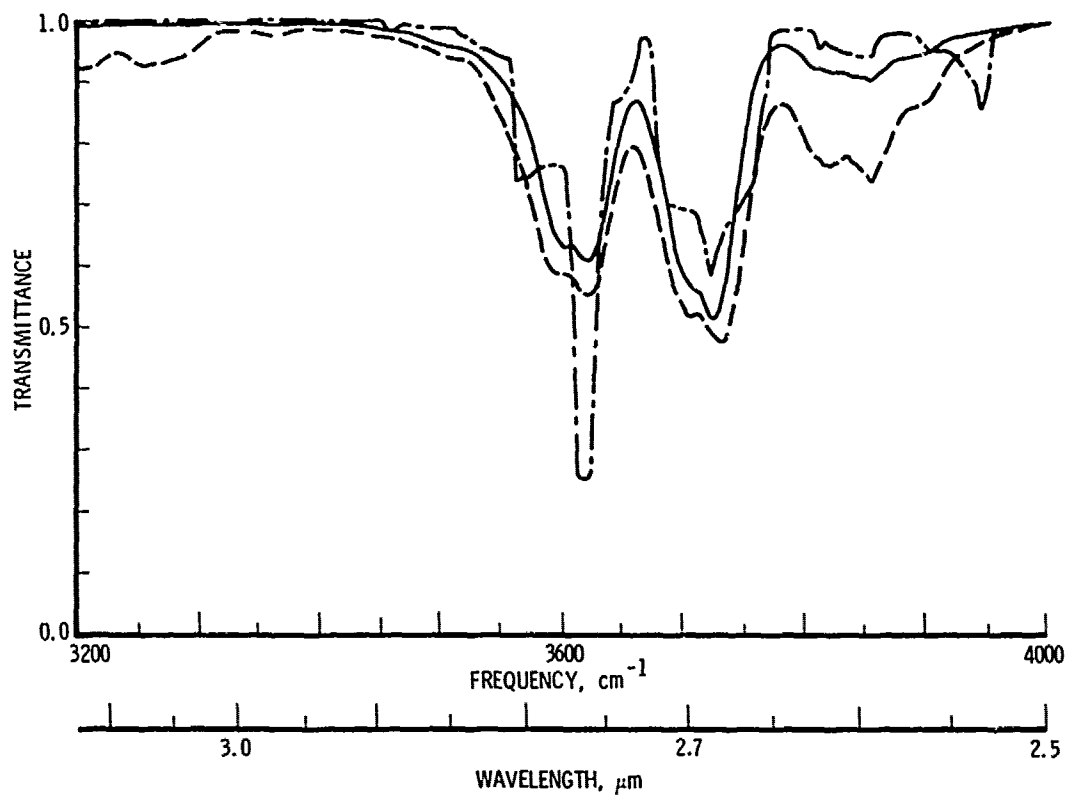


Figure 36. Dependence of Apparent Transmittance on Source Spectrum Between 3200 and 4000 cm^{-1} . The solid curve denotes the average transmittance at 20 cm^{-1} resolution from Fig. 26. The dashed curve is the effective average transmittance for Plume A, which is the ratio of the 20 cm^{-1} resolution curve of Fig. 30 to that of Fig. 28. The broken curve denotes the effective average transmittance for Plume B, which is the ratio of the 20 cm^{-1} resolution spectrum from Fig. 34 to that of Fig. 32.

$$\bar{T}_e = \frac{\int_{\Delta\nu} L(\nu) \tau(\nu) d\nu}{\int_{\Delta\nu} L(\nu) d\nu}$$

where $L(\nu)$ is the source radiance, and $\tau(\nu)$ is the atmospheric transmittance, both at infinite resolution. \bar{T}_e is essentially the ratio of the 20-cm^{-1} resolution apparent radiance curve to the appropriate 20-cm^{-1} resolution plume radiance.

The accuracy of spectra presented in this section is limited by several approximations in addition to the validity of the plume models for any real system. As demonstrated in Section II, the AFCRL line atlas is not completely adequate for modeling hot gases. DF and DCI have been omitted from the plume B computations. The pressures for the gas samples are on the border line of the validity of the pressure-broadened Lorentz line shape. A Voigt line shape was not used because of the additional computer expense.

REFERENCES

1. C. M. Randall, Monochromatic Transmittance/Radiance Computations, IR-0075(5647)-3, The Aerospace Corporation, El Segundo, Calif. (31 December 1974).
2. R. A. McClatchey et al., AFCRL Atmospheric Absorption Line Parameters Compilation, Paper 434, AFCRL-TR-73-0096, Air Force Cambridge Research Laboratories, Cambridge, Mass. (26 January 1973).
3. D. E. Burch, D. A. Gryvnak, and R. R. Patty, Absorption by CO₂ Between 3100 and 4100 cm⁻¹ (2.44 - 3.22 Microns), U-4132, Aeronutronic Division, Philco-Ford, Newport Beach, Calif. (30 April 1968).
4. D. E. Burch, D. A. Gryvnak, and R. R. Patty, Absorption by H₂O Between 2800 and 4500 cm⁻¹ (2.7 Micron Region), U-3202, Aeronutronic Division, Philco-Ford, Newport Beach, Calif. (30 September 1965).
5. F. S. Simmons, H. Y. Yamada, and C. B. Arnold, Measurements of Temperature Profiles in Hot Gases by Emission-Absorption Spectroscopy, Report WRL 8962-18-F, NASA CR-72491, University of Michigan, Willow Run Laboratories, Ann Arbor, Mich. (April 1969).
6. D. E. Burch and D. A. Gryvnak, Infrared Radiation Emitted by Hot Gases and its Transmission Through Synthetic Atmospheres, U-1929, Aeronutronic Division, Philco-Ford, Newport Beach, Calif. (30 October 1962).
7. F. S. Simmons, C. B. Arnold, and D. H. Smith, Studies of Infrared Radiative Transfer in Hot Gases 1: Spectral Absorptance Measurements in the 2.7 μ H₂O Bands, Report 4613-91-T, University of Michigan, Willow Run Laboratories, Ann Arbor, Mich. (August 1965).
8. Gerhard Herzberg, Molecular Spectra and Molecular Structure, I Spectra of Diatomic Molecules, Van Nostrand, New York (1950).
9. D. E. Mann, B. A. Thrush, D. R. Lide, Jr., J. J. Ball, and N. Acquista, "Spectroscopy of Fluorine Flames. I. Hydrogen - Fluorine Flame and the Vibration-Rotation Emission Spectrum of HF," J. Chem. Phys. 34, 420 (1961).

10. D. H. Rank, B. S. Rao, and T. A. Wiggins, "Molecular Constants of HCl^{35} ," J. Mol. Spectr. **17**, 122 (1965).
11. J. L. Dunham, "The Energy Levels of a Rotating Vibrator," Phys. Rev. **41**, 721 (1932).
12. L. A. Young and W. J. Eachus, "Dipole Moment Function and Vibration-Rotation Matrix Elements for CO," J. Chem. Phys. **44**, 4195 (1966).
13. R. E. Meredith and F. G. Smith, "Computation of Electric Dipole Matrix Elements for Hydrogen Fluoride," J. Quant. Spectr. Radiative Transfer **13**, 89 (1973).
14. F. G. Smith, "Dipole Moment Function and Vibration-Rotation Matrix Elements for HCl^{35} and DCl^{35} ," J. Quant. Spectr. Radiative Transfer **13**, 717 (1973).
15. R. Herman and R. F. Wallis, "Influence of Vibration-Rotation Interaction on Line Intensities in Vibration-Rotation Bands of Diatomic Molecules," J. Chem. Phys. **23**, 637 (1955).
16. R. E. Meredith and N. F. Kent, Line-Strength Calculations for the 0-1, 0-2, 0-3, and 1-2 Vibration-Rotation Bands of Hydrogen Fluoride, Report 4613-125-T, University of Michigan, Willow Run Laboratories, Ann Arbor, Mich. (April 1966).
17. R. E. Meredith, Matrix Elements for the 0-3, 2-3, 3-4 Vibration-Rotation Bands of Diatomic Molecules, Report 4613-138-T, University of Michigan, Willow Run Laboratories, Ann Arbor, Mich. (February 1967).
18. W. S. Benedict, R. Herman, G. E. Moore, and S. Silverman, "The Strengths, Widths, and Shapes of Infrared Lines II. The HCl Fundamental," Can. J. Phys. **34**, 850 (1956).
19. E. Lindholm, Z. Phys. **113**, 596 (1939).
20. H. Goldring and W. Benesch, "Widths of HCl Overtone Lines at Various Temperatures," Can. J. Phys. **40**, 1801 (1962).
21. H. Babrov, G. Ameer, and W. Benesch, "Molecular Collision Cross Sections from Infrared Absorption Measurements," J. Chem. Phys. **33**, 145 (1960).
22. D. F. Smith, "The Overlapping Hydrogen Fluoride Monomer-Dimer Spectra," J. Mol. Spectr. **3**, 473 (1959).

23. B. M. Shaw and R. J. Lovell, "Foreign-Gas Broadening of HF by CO₂," J. Opt. Soc. Am. 59, 1598 (1969).
24. D. U. Webb and K. N. Rao, "A Heated Absorption Cell for Studying Infrared Absorption Bands," Appl. Opt. 5, 1461 (1966).
25. W. S. Benedict, R. Herman, G. E. Moore, and S. Silverman, "Infrared Line and Band Strengths and Dipole Moment Function in HCl and DCl," J. Chem. Phys. 26, 1671 (1957).
26. R. J. Lovell and W. F. Herget, "Lorentz Parameters and Vibration-Rotation Interaction Constants for the Fundamental Band of HF," J. Opt. Soc. Am. 52, 1374 (1962).
27. G. A. Kuipers, "The Spectrum of Monomeric Hydrogen Fluoride: Line Shapes, Intensities, and Breadths," J. Mol. Spectr. 2, 75 (1958).
28. R. E. Meredith, "Strengths and Widths in the First Overtone Band of Hydrogen Fluoride," J. Quant. Spectr. Radiative Transfer 12, 485 (1972).
29. P. W. Anderson, "Pressure Broadening in the Microwave and Infrared Regions," Phys. Rev. 76, 647 (1949).
30. A. Goldman, S. C. Schmidt, J. R. Riter, and R. M. Blunt, "Infrared Spectral Radiance of Hot HF and DF in the $\Delta v=1$ Bands Region as Seen through an Atmospheric Path," J. Quant. Spectr. Radiative Transfer 14, 299 (1974).
31. R. A. McClatchey, R. W. Fenn, J. E. A. Selby, F. E. Volz, and J. S. Garing, Optical Properties of the Atmosphere (Third Ed.), Paper No. 411, AFCRL-72-0497, Air Force Cambridge Research Laboratories, Cambridge, Mass. (24 August 1972).

APPENDIX. LINE PARAMETERS FOR HCl^{35} , HCl^{37} , AND HF

The line parameters calculated as described in the text for $T = 296 \text{ K}$ are listed in Table A-1 in order of increasing frequency. Listed are all lines of the 0-1, 1-2, 2-3, 3-4, and 0-2 bands of HCl^{35} , HCl^{37} , and HF with strengths such that at 3000 K, a 1-m path of pure gas at atmospheric pressure would have an absorption of 1 percent or greater. The format of the computer listing of each line is defined in Table A-2.

2485.277	3.133	-25	.063	3891.929	1	0	0	12	74	15	3
2486.434	1.942	-27	.127	3023.799	4	3	0	12	74	17	3
2486.817	1.440	-23	.133	7189.702	3	3	0	8	74	15	3
2487.823	5.666	-37	.127	3030.649	4	3	0	12	74	15	3
2410.534	5.264	-59	.100	20148.997	4	3	0	22	74	19	3
2420.430	1.734	-29	.050	5283.216	2	1	1	15	74	17	3
2421.814	5.088	-29	.050	5288.854	2	1	1	15	74	15	3
2421.891	1.853	-55	.130	18478.539	2	2	1	24	74	19	7
2427.460	3.245	-52	.100	16889.173	3	2	1	26	74	19	7
2427.494	2.341	-49	.100	15375.715	1	1	0	28	74	19	7
2428.467	3.403	-25	.050	3504.245	1	1	0	18	74	17	3
2429.299	3.593	-37	.153	8872.500	4	3	0	7	74	17	3
2429.441	1.884	-25	.050	3509.447	1	1	0	18	74	15	3
2430.726	1.023	-36	.153	8879.134	4	3	0	7	74	15	3
2430.927	2.203	-33	.084	6951.270	3	3	2	11	74	17	3
2432.245	1.525	-32	.084	6957.211	3	2	2	11	74	15	3
2447.744	1.762	-29	.050	4986.527	3	2	1	14	74	17	3
2449.172	1.388	-28	.050	4991.734	2	2	1	14	74	15	3
2451.145	1.888	-37	.186	8730.911	4	3	3	6	74	17	3
2453.119	1.651	-35	.186	8746.345	4	3	3	6	74	15	3
2455.556	1.317	-32	.050	6737.945	3	3	3	10	74	17	3
2457.214	3.865	-32	.090	6743.578	3	3	2	10	74	15	3
2457.513	1.496	-25	.060	3141.061	1	1	0	17	74	17	3
2459.037	1.031	-24	.060	3145.732	1	1	0	17	74	15	3
2465.555	1.599	-57	.130	19423.926	4	3	3	21	74	19	7
2473.434	2.777	-37	.227	4627.986	4	3	3	5	74	17	3
2474.537	2.392	-28	.056	4708.790	2	1	1	13	74	17	3
2474.989	2.163	-36	.227	4632.367	4	3	1	5	74	15	3
2476.110	2.048	-28	.056	4713.592	2	1	1	13	74	15	3
2479.423	3.946	-54	.189	17569.465	3	3	2	33	74	19	7
2480.213	3.088	-52	.186	6543.586	3	3	2	9	74	17	3
2481.710	3.841	-32	.186	6548.938	3	3	2	9	74	15	3
2486.379	1.733	-24	.050	2796.837	1	1	0	16	74	17	3
2487.230	3.781	-53	.189	15991.289	3	3	1	25	74	19	7
2487.451	1.231	-24	.050	2801.913	1	1	0	16	74	15	3
2489.452	3.302	-47	.100	14395.721	4	3	0	27	74	19	7
2494.733	1.011	-35	.246	8531.128	1	1	4	4	74	17	3
2496.324	2.351	-35	.246	4537.274	4	4	3	4	74	15	3
2501.097	1.581	-28	.083	4450.173	2	2	1	12	74	17	3
2502.513	2.362	-27	.083	4454.598	2	2	1	12	74	15	3
2504.195	1.944	-32	.127	5368.315	3	3	2	8	74	17	3
2505.721	1.810	-31	.127	5374.542	3	3	2	8	74	15	3
2514.751	1.793	-24	.050	2471.777	1	1	0	15	74	17	3
2515.551	1.182	-35	.249	8455.089	4	4	3	3	74	17	3
2516.277	2.199	-23	.050	2475.465	1	1	0	15	74	15	3
2517.110	3.178	-36	.249	9461.126	4	4	3	3	74	15	3
2520.440	4.892	-56	.100	10723.719	4	4	3	20	74	19	7
2527.110	2.318	-27	.084	4210.835	2	2	1	11	74	17	3
2527.551	1.139	-31	.153	6212.240	2	2	1	7	74	17	3
2528.559	1.559	-27	.084	4214.939	3	3	2	11	74	15	3
2529.234	3.356	-31	.153	5217.111	3	3	2	7	74	15	3
2535.747	1.738	-37	.223	8798.018	4	4	3	2	74	17	3
2536.679	1.736	-32	.153	15888.348	4	4	3	2	74	19	7
2537.335	1.749	-35	.223	8403.972	4	4	3	2	74	15	3
2542.715	3.174	-23	.050	2166.075	4	4	0	14	74	17	3
2544.280	9.425	-23	.050	2169.312	1	0	0	14	74	15	3

29442
 29443
 29444
 29445
 29446
 29447
 29448
 29449
 29450
 29451
 29452
 29453
 29454
 29455
 29456
 29457
 29458
 29459
 29460
 29461
 29462
 29463
 29464
 29465
 29466
 29467
 29468
 29469
 29470
 29471
 29472
 29473
 29474
 29475
 29476
 29477
 29478
 29479
 29480
 29481
 29482
 29483
 29484
 29485
 29486
 29487
 29488
 29489
 29490
 29491
 29492
 29493
 29494
 29495
 29496
 29497
 29498
 29499
 29500
 29501
 29502
 29503
 29504
 29505
 29506
 29507
 29508
 29509
 29510
 29511
 29512
 29513
 29514
 29515
 29516
 29517
 29518
 29519
 29520
 29521
 29522
 29523
 29524
 29525
 29526
 29527
 29528
 29529
 29530
 29531
 29532
 29533
 29534
 29535
 29536
 29537
 29538
 29539
 29540
 29541
 29542
 29543
 29544
 29545
 29546
 29547
 29548
 29549
 29550
 29551
 29552
 29553
 29554
 29555
 29556
 29557
 29558
 29559
 29560
 29561
 29562
 29563
 29564
 29565
 29566
 29567
 29568
 29569
 29570
 29571
 29572
 29573
 29574
 29575
 29576
 29577
 29578
 29579
 29580
 29581
 29582
 29583
 29584
 29585
 29586
 29587
 29588
 29589
 29590
 29591
 29592
 29593
 29594
 29595
 29596
 29597
 29598
 29599
 29600

29601
 29602
 29603
 29604
 29605
 29606
 29607
 29608
 29609
 29610
 29611
 29612
 29613
 29614
 29615
 29616
 29617
 29618
 29619
 29620
 29621
 29622
 29623
 29624
 29625
 29626
 29627
 29628
 29629
 29630
 29631
 29632
 29633
 29634
 29635
 29636
 29637
 29638
 29639
 29640
 29641
 29642
 29643
 29644
 29645
 29646
 29647
 29648
 29649
 29650
 29651
 29652
 29653
 29654
 29655
 29656
 29657
 29658
 29659
 29660
 29661
 29662
 29663
 29664
 29665
 29666
 29667
 29668
 29669
 29670
 29671
 29672
 29673
 29674
 29675
 29676
 29677
 29678
 29679
 29680
 29681
 29682
 29683
 29684
 29685
 29686
 29687
 29688
 29689
 29690
 29691
 29692
 29693
 29694
 29695
 29696
 29697
 29698
 29699
 29700

29701
 29702
 29703
 29704
 29705
 29706
 29707
 29708
 29709
 29710
 29711
 29712
 29713
 29714
 29715
 29716
 29717
 29718
 29719
 29720
 29721
 29722
 29723
 29724
 29725
 29726
 29727
 29728
 29729
 29730
 29731
 29732
 29733
 29734
 29735
 29736
 29737
 29738
 29739
 29740
 29741
 29742
 29743
 29744
 29745
 29746
 29747
 29748
 29749
 29750
 29751
 29752
 29753
 29754
 29755
 29756
 29757
 29758
 29759
 29760
 29761
 29762
 29763
 29764
 29765
 29766
 29767
 29768
 29769
 29770
 29771
 29772
 29773
 29774
 29775
 29776
 29777
 29778
 29779
 29780
 29781
 29782
 29783
 29784
 29785
 29786
 29787
 29788
 29789
 29790
 29791
 29792
 29793
 29794
 29795
 29796
 29797
 29798
 29799
 29800

29801
 29802
 29803
 29804
 29805
 29806
 29807
 29808
 29809
 29810
 29811
 29812
 29813
 29814
 29815
 29816
 29817
 29818
 29819
 29820
 29821
 29822
 29823
 29824
 29825
 29826
 29827
 29828
 29829
 29830
 29831
 29832
 29833
 29834
 29835
 29836
 29837
 29838
 29839
 29840
 29841
 29842
 29843
 29844
 29845
 29846
 29847
 29848
 29849
 29850
 29851
 29852
 29853
 29854
 29855
 29856
 29857
 29858
 29859
 29860
 29861
 29862
 29863
 29864
 29865
 29866
 29867
 29868
 29869
 29870
 29871
 29872
 29873
 29874
 29875
 29876
 29877
 29878
 29879
 29880
 29881
 29882
 29883
 29884
 29885
 29886
 29887
 29888
 29889
 29890
 29891
 29892
 29893
 29894
 29895
 29896
 29897
 29898
 29899
 29900

Table A-2. Format of Spectroscopic Line Atlas Listing

Characters	FORTRAN Format	Parameter	Units
1 - 10	F10.3	Line center frequency	cm^{-1}
11 - 20	E10.3	Line strength at 296 K	$\text{cm}^{-1}/$ (molecule $\cdot \text{cm}^{-2}$)
21 - 25	F5.3	Line-width parameter at 273 K	$\text{cm}^{-1}/\text{atmosphere}$
26 - 35	F10.3	Energy level of lower state in transition	cm^{-1}
36 - 44	Blank		
45	I1	Vibrational quantum number of upper state	None
46 - 56	Blank		
57	I1	Vibrational quantum number of lower state	None
58 - 65	Blank		
66	A1	Rotational branch	None
67 - 69	I3	Rotational quantum number of lower state	None
70,71	Blank		
72,73	I2	"74" for date	None
74,75	Blank		
76,77	I2	Isotope 15 HCl ³⁵ 17 HCl ³⁷ 19 HF	None
78,79	Blank		
80	I1	Molecule 3 HCl 7 HF	None

LABORATORY OPERATIONS

The Laboratory Operations of The Aerospace Corporation is conducting experimental and theoretical investigations necessary for the evaluation and application of scientific advances to new military concepts and systems. Versatility and flexibility have been developed to a high degree by the laboratory personnel in dealing with the many problems encountered in the nation's rapidly developing space and missile systems. Expertise in the latest scientific developments is vital to the accomplishment of tasks related to these problems. The laboratories that contribute to this research are:

Aerophysics Laboratory: Launch and reentry aerodynamics, heat transfer, reentry physics, chemical kinetics, structural mechanics, flight dynamics, atmospheric pollution, and high-power gas lasers.

Chemistry and Physics Laboratory: Atmospheric reactions and atmospheric optics, chemical reactions in polluted atmospheres, chemical reactions of excited species in rocket plumes, chemical thermodynamics, plasma and laser-induced reactions, laser chemistry, propulsion chemistry, space vacuum and radiation effects on materials, lubrication and surface phenomena, photo-sensitive materials and sensors, high precision laser ranging, and the application of physics and chemistry to problems of law enforcement and biomedicine.

Electronics Research Laboratory: Electromagnetic theory, devices, and propagation phenomena, including plasma electromagnetics; quantum electronics, lasers, and electro-optics; communication sciences, applied electronics, semi-conducting, superconducting, and crystal device physics, optical and acoustical imaging; atmospheric pollution; millimeter wave and far-infrared technology.

Materials Sciences Laboratory: Development of new materials; metal matrix composites and new forms of carbon; test and evaluation of graphite and ceramics in reentry; spacecraft materials and electronic components in nuclear weapons environment; application of fracture mechanics to stress corrosion and fatigue-induced fractures in structural metals.

Space Physics Laboratory: Atmospheric and ionospheric physics, radiation from the atmosphere, density and composition of the atmosphere, aurorae and airglow; magnetospheric physics, cosmic rays, generation and propagation of plasma waves in the magnetosphere; solar physics, studies of solar magnetic fields; space astronomy, x-ray astronomy; the effects of nuclear explosions, magnetic storms, and solar activity on the earth's atmosphere, ionosphere, and magnetosphere; the effects of optical, electromagnetic, and particulate radiations in space on space systems.

THE AEROSPACE CORPORATION
El Segundo, California